Fuel 224 (2018) 147–166

Contents lists available at ScienceDirect

Fuel

journal homepage: www.elsevier.com/locate/fuel

Full Length Article

The effect of Aluminum oxide nanoparticles addition with Jojoba methyl ester-diesel fuel blend on a diesel engine performance, combustion and emission characteristics

Ahmed I. El-Seesy*, Ali M.A. Attia, Hesham M. El-Batsh

Mechanical Engineering Department, Benha Faculty of Engineering, Benha University, 13512 Benha, Qalubia, Egypt

ARTICLE INFO

Keywords:
Jojoba methyl ester
Alumina nanoparticles
Diesel engine
Heat release rate
Engine performance
Emission characteristics

ABSTRACT

In the current work, an experimental investigation was conducted to recommend the optimal concentration of alumina nanoparticles (Al_2O_3) into Jojoba biodiesel-diesel (JB20D) fuel blend at which the best diesel engine performance and exhaust emissions were attained. The Al_2O_3 nanoparticles with concentrations varied from 10 to 50 mg/l by step of 10 mg/l were mixed into JB20D fuel blend with the help of ultrasonic stabilization. The results of the present study revealed that JB20D slightly reduced the engine performance and increased its emission characteristics at all engine tested operating conditions as compared to pure diesel oil. Utilizing of Al_2O_3 additives was found to improve all engine performance characteristics. However, the best emission characteristics were obtained at the dose level of 20 mg/l, where remarkable emissions reduction were observed; NO_x by 70%, CO by 80%, UHC by 60%, and Smoke opacity by 35%. While the best of both mechanical performance and engine combustion characteristics were achieved at a concentration of 40 mg/l, where the reduction in the brake specific fuel consumption – bsfc was by 12% and increase in the cylinder peak pressure – p_{max}, the maximum rate of pressure rise – $dp/d\theta_{max}$, and maximum rate of gross heat release – $dQ_g/d\theta_{max}$ were 4.5%, 4%, and 4%, respectively. According to the comparisons of engine performance and emissions, the recommended concentration of Al_2O_3 in JB20D blends was concluded to be 30 mg/l, which gave remarkable enhancement in all engine performance parameters.

1. Introduction

Compression ignition engines play a substantial role in transportation, locomotives, irrigation sector and industrial sectors due to their simplicity of operation, high reliability, durability and well-established design. On the other hand, diesel engines are considered one of the primary sources of many toxic emissions, especially, the particulate matter (PM), and nitrogen oxides (NO_x) which have hazardous environmental impacts. These toxic compounds cause the formation of acidic rains, the depletion of ozone layer, the increase of greenhouse phenomena, the formation of smog, and undesirable climatic changes [1–3]. There are essential approaches to reduce diesel emissions; including engine design modifications, engine combustion enhancement, and the use of exhaust gas treatment tools [4]. The modification of engine combustion seems to be the most recommended because it may need only minor changes to engine systems rather than the use of new designs or the use of additional systems. This approach is realized by regulating the fuel properties, modifying fuel injection, and use of fuel additives [4,5]. In this regard, the use of oxygenated fuels as biodiesel is found to be a promising alternative to substitute the conventional diesel fuel. Thus, the alternative fuels would depend on renewable resources. Currently, the most promising renewable fuel resource is the use of biomass to produce the commonly called biofuels. On the other hand, to completely overcome additional problems related to food requirements around the world, the proposed biomass resources shall be non-edible [4,6]. The most recommended non-edible oils are those generated from plants that do not need a significant amount of water or can grow in the barren lands using waste-water [4,6,7]. These generated fuels will support nations to reduce the import of fossil fuels or extend the time until the depletion of the current fuel reserves [4].

Jojoba is a name that is becoming increasingly common as an industrial crop in several countries. In recent years, Jojoba oil has become the most genuinely Egyptian product [8]. Jojoba plant is one of the promising non-edible plants growing in the desert. Also, its seed has more than 50% of its weight as raw oil. Thus, raw Jojoba oil would be suitable feedstock for biodiesel production. Furthermore, the choice of

* Corresponding author.
E-mail addresses: ahmed.elsisi@ejust.edu.eg, ahmed.elsysy@bhit.bu.edu.eg, eng.elseesy@gmail.com (A.I. El-Seesy).
URL: http://beng.bu.edu.eg/beng/en/ (A.I. El-Seesy).

https://doi.org/10.1016/j.fuel.2018.03.076
Received 20 June 2017; Received in revised form 7 March 2018; Accepted 13 March 2018

Nomenclature

ASTM	American Society for Testing and Materials
ATDC	after top dead center
CA	crank angle, degree
CO	carbon monoxide, ppm
D100	pure diesel oil
EGT	exhaust gas temperature, ˚C
EVC	exhaust valve closed
EVO	exhaust valve opened
h_c	heat transfer coefficient, w/m^2.k
IVC	inlet valve closed
Al_2O_3	Aluminum oxide
JME	Jojoba methyl ester
JB20D	blended fuel containing 20% JME + 80% D100
JB20D10A	blended fuel (JB20D) + 10 mg/l of Aluminum oxide
JB20D20A	blended fuel (JB20D) + 20 mg/l of Aluminum oxide
JB20D30A	blended fuel (JB20D) + 30 mg/l of Aluminum oxide
JB20D40A	blended fuel (JB20D) + 40 mg/l of Aluminum oxide
JB20D50A	blended fuel (JB20D) + 50 mg/l of Aluminum oxide
N	engine speed, rpm
NO_x	nitrogen oxides, ppm
p	instantaneous cylinder pressure, bar
T	mean gas temperature, K
T_w	wall temperature, K
UHC	unburned hydrocarbons, %
V	instantaneous cylinder volume, m^3
$dp/d\theta$	pressure rise rate per crank angle, bar/deg.
$dV/d\theta$	volume rise rate per crank angle, m^3/deg.
$dQ_g/d\theta$	gross heat release rate per crank angle, J/deg.
θ	crank angle, deg.
γ	specific heat ratio

the Egyptian Jojoba oil (GREEN GOLD) is due to its availability in Egypt, its low price, and its low chemical reactivity [8,9]. From the literature, most of the studies used various methods for extraction of Jojoba oil from the seeds [10]. Those techniques are mainly mechanical pressing, mechanical pressing followed by solvent extraction, or solvent extraction only. Jojoba oil is primarily composed of straight-chain wax esters in the range of C_{26}–C_{48} with two double bonds, one at each side of the ester bond. It is not a triglyceride, making Jojoba and its derivative Jojoba esters more similar to sebum and whale oil than traditional vegetable oils [11]. The raw Jojoba oil is converted into biodiesel via transesterification process to receive Jojoba Methyl Ester (JME). It has many advantages as it performs under normal conditions and yields better quality biodiesel [11].

A few researchers examined the utilization of Jojoba oil as an alternative engine fuel. They emphasized the suitability of such promising fuel for diesel engines [12–14]. However, as reported by many researchers [15,16], the usage of Jojoba oil in the diesel engine decrease the engine thermal efficiency, increase the specific fuel consumption and increase the engine emissions, especially the NO_x emissions. Shehata and Abdel Razek [15], Huzayyin et al. [16], Saleh [17] and Al-Widyan et al. [18] investigated the performance and emissions of the diesel engine fueled by sunflower (S100) and blend of 20% Jojoba oil plus 80% pure diesel fuel (B20). The results showed that the brake thermal efficiency was reduced due to the lower heating value of S100 and B20 compared to diesel fuel. Also, they found that the CO and NO_x emissions were increased for both S100 and B20 compared to pure diesel fuel.

Currently, there is considerable attention to utilizing nanoparticles-additives to improve the combustion quality of the burned fuel. Metallic based and oxygen-containing compounds, such as Aluminum oxide (Al_2O_3), Titanium oxide (TiO_2), Copper oxide (CuO), and others which act as a combustion catalyst for hydrocarbon fuels [19], [20]. These additives enhanced the radiative mass transfer properties, reduced ignition delay and improved the ignition temperature parameters of the fuel within the combustion zone [21]. For engine applications, there are many trials to study the effect of nano-additives on engine performance. Accordingly, some experimental investigations were conducted with the use of nano-additives blends with biodiesel and diesel fuel to improve the fuel properties and engine performance, as well as to reduce the engine emissions [22–24].

Ganesh and Gowrishankar [25] studied the effects of the addition of Magnalium and Cobalt Oxide nanoparticles on diesel engine performance fueled by Jatropha biodiesel. They found that the addition of nanoparticles resulted in a significant improvement in the brake thermal efficiency and reduction in the bsfc by 2%. Also, the emissions have remarkable reduction where UHC was reduced by 60%, CO by 50% and the NO_x by 45%. Moreover, Solero [26] examined the effects of adding Al_2O_3 nanoparticles on the combustion characteristics of diesel fuel spray. He found that the addition of Al_2O_3 with a concentration of 0.1% by volume to diesel fuel improved the combustion characteristics of the fuel spray, and reduced the level of CO emission. In addition, Gürü et al. [27] studied the improvement of diesel fuel properties utilizing additives of organic compounds of Mn, Mg, Cu and Ca with different concentrations of 13.5, 27.1, 54.2, and 94.9 μmol/l blended fuel. The results showed that the Mn had the significant reduction in the fuel freezing point, while the cetane number was increased by about 5%. The CO emission was decreased by 14.3%, and the brake thermal efficiency was increased by 0.8%.

Furthermore, Selvan et al. [28], Sajeevan and Sajith [29] and Sajith et al. [30] investigated the impacts of Cerium oxide additives in diesel and diesel-biodiesel-ethanol blends on the diesel engines performance. They found that the addition of nanoparticles into diesel-biodiesel-ethanol blends decreased the specific fuel consumption, increased the peak pressure and shortened the ignition delay. The addition of Cerium oxide also accelerated earlier initiation of combustion and caused a lower heat release rate. Emissions of CO, UHC, and NO_x were significantly reduced. They also reported that the optimum engine performance was achieved at nanoparticles dose level of 35 ppm.

Kao et al. [31], Aalam and Saravanan [32] and Basha and Anand [33–35] also examined the effects of adding Aluminium (Al) nanoparticles and Aluminium oxide (Al_2O_3) with diesel, biodiesel, emulsified diesel fuel, and emulsified biodiesel fuel on a diesel engine performance. They found that the peak pressure, pressure rise rate, heat release rate, and the brake specific fuel consumption were reduced. The NO_x, CO, UHC, and soot emissions were remarkably reduced due to the addition of nanoparticles.

In another experimental investigation, Tyagi et al. [36] studied the effects of the addition Aluminium (Al) and Al_2O_3 nanoparticles on the ignition characteristics of diesel fuel. They found that the radiative and heat/mass transfer properties of diesel fuel were enhanced remarkably. They also reported that the hot plate ignition probability of the diesel fuel increased significantly. Also, Gan and Qiao [37] studied the impacts of the addition of nano and micron-sized Aluminum (Al) particles on combustion characteristics of n-decane and ethanol droplets by varying its size, dispersant concentration, and type of base fluid. They found that the engine power was remarkably enhanced. They also reported that the CO_2 and NO_x emissions were significantly reduced.

Mehta et al. [38] studied the engine performance and emission characteristics of a diesel engine operated with diesel fuel with the addition of Aluminum and Iron nanoparticles. They found that the peak cylinder pressures and the brake thermal efficiency were increased by 4% and 9%, respectively while the bsfc was decreased by 7%. Engine emissions of CO and UHC were reduced by 40%, and 8% respectively. Kannan et al. [39] examined the effects of ferric chloride ($FeCl_3$)

additives into biodiesel on the diesel engine performance and emissions characteristics. They found that the bsfc was decreased by 8.6%, while the brake thermal efficiency was increased by 6.3%. They also reported that the cylinder pressure and heat release rate were increased. Emissions of CO, UHC, NO_x, and smoke were reduced by 52.6%, 26.6%, 21.5% and 6.9%, respectively.

Furthermore, Venu et al. [40] examined the effects of adding Alumina (Al_2O_3) nanoparticles with biodiesel-diesel-ethanol blends on a diesel engine performance and emissions. They found that the combustion characteristics were significantly improved. Emissions of UHC, CO, NO_x, and smoke were remarkably reduced. Also, Gumus et al. [41] studied the influences of adding Aluminium oxide (Al_2O_3) and Copper oxide (CuO) nanoparticles to diesel fuel on diesel engine performance and emissions. They found that the flash point and cetane index were increased. The authors also concluded that the engine torque and power were increased by 1% and 3.3%, respectively. Engine emissions of CO, UHC, and NO_x were significantly reduced by 11%, 13%, and 6%, respectively.

From the literature survey, it can be concluded that nanoparticles have a significant positive effect in improving combustion characteristics. Recently, few studies were found concerning an experimental investigation of the engine performance and emissions of the nano-additive-blended biodiesel-diesel mixture. Therefore, the main aim of this work is to compare the engine performance, combustion and emissions characteristics of the recommended Jojoba biodiesel-blended diesel fuel (JB20D) without and with the AL_2O_3 additives at different engine speeds and loads to obtain the optimum concentration of nanoparticles. The Al_2O_3 were added to the JB20D at five different dose levels of 10, 20, 30, 40 and 50 mg/l. The combustion characteristics parameters, such as cylinder pressure, pressure rise rate, gross heat release rate, ignition delay and mass fraction of burned fuel were considered. The engine performance parameters, such as brake thermal efficiency (BTE), brake specific fuel consumption (bsfc) and exhaust gas temperature (EGT) as well as CO, NO_x, UHC emissions and smoke opacity were also examined.

2. Experimental setup and procedures

The specifications of the test rig which was utilized in this study are shown in Table 1. The whole experimental layout equipped with the necessary instruments to measure the different engine parameters is shown in Fig. 1. The DC generator (MODEL, MEZ-BURNO, 10.5 kW) is coupled to the diesel engine to measure the engine brake power. The electric heaters within flowing water are used to consume the power of the generator. Thus, an external controllable excitation electrical circuit consisting of an AC autotransformer (Variac) and a rectifier bridge is used to supply the DC generator with the magnetic field. The load values are chosen and defined by selecting the generator excitation voltage values using the autotransformer.

The engine brake power was determined by measuring output voltage and current from the DC generator. The fuel consumption was measured by recording the time needed to consume a specific volume of the test fuel contained in a graduated glass jar. The intake airflow rate was measured as the flow throughout laminar flow element (MERIAM-50MC2) entering a damping air box of 0.45 m^3. The engine speed was measured by using the digital optical tachometer (Pioneered Electrical & Research Corporation, Model DS-303). Temperature measurements were carried out at various locations in the experimental set-up; including the temperature of ambient air, intake air, oil, exhaust, and cylinder wall. For this purpose, five calibrated thermocouple props of type (K) were adjusted in these positions. A selecting switch (type omega) is used to change among these thermocouples, and any reading is read out by a digital thermometer (Omega-Model 650).

The CO, CO_2, O_2, NO_x and UHC emissions are measured by using AVL Dicom 4000-NO_x self-calibrated exhaust analyzer. The smoke opacity was measured using opacity chamber Model AVL DiSmoke 4000. The technical specifications for gas analyzer are shown in Table 2.

The cylinder pressure was measured by a Kistler piezoelectric pressure sensor (Model 6061B of pressure range up to 250 bar and sensitivity ≈ −27.5 pc/bar) connected with Kistler charge amplifier (Model 5018A). The crank angle encoder of Model LM12-3004NA (at detecting distance of 4 mm supplied with DC voltage up to 36 V) was adjusted to work effectively at the location of piston top dead center (TDC). The location of TDC was detected with the help of a digital linear displacement relative to the position of the proximity (SONY-MAGNESCALE-LY-1115, the sensitivity of 5 μm). Both signals from charge amplifier and the proximity sensor are converted from analog to digital data via Data-Acquisition Card (DAQ Model NI PCI-6251with terminal block SCB-68) that is installed on PC and controlled by LabVIEW software.

2.1. Heat release rate model

A single zone combustion model is utilized in this work in order to understand the phenomena that occur during a combustion cycle, from the intake fuel entry to the end of exhaust operation. The net heat release rate ($dQ_{net}/d\theta$) and heat transfer to cylinder wall ($dQ_{wall}/d\theta$) are primary parameters. These parameters were calculated using the measured cylinder pressure p(θ). Thus, the gross heat release rate was calculated using first law-single zone model equation as follows [42].

$$\frac{dQ_{gross}}{d\theta} = \frac{\gamma_{(T)}}{\gamma_{(T)}-1} \times p \times \frac{dV}{d\theta} + \frac{1}{\gamma_{(T)}-1} \times V \times \frac{dp}{d\theta} + \frac{dQ_{wall}}{d\theta} \quad (1)$$

The specific heat ratio γ(T) influences the shape, and the peak of the heat release rate, γ (T) of the gases was calculated using the following equation [22]:

$$\gamma_{(T)} = 1.35-6 \times 10^{-5} \times T + 10^{-8} \times T^2 \quad (2)$$

With the help of the measured cylinder pressure and the calculated cylinder volume, the gas temperature (T) was calculated using the equation of state as follows [43].

$$T = \frac{T_r \times p \times V}{p_r \times V_r} \quad (3)$$

All thermodynamic states (P_r, T_r, V_r) were evaluated at a given reference condition such as IVC (P_{IVC}, T_{IVC}, V_{IVC}). T_{IVC} and P_{IVC} were temperature/pressure at IVC and equal 350 K, and $1.013 * 10^5$ Pa respectively.

The rate of heat transfer from gases to cylinder wall was calculated using convection heat transfer equation as follows [42].

$$\frac{dQ_{wall}}{d\theta} = h_C \times A(\theta) \times (T-T_{wall}) \quad (4)$$

Table 1
Technical specifications of the test engine.

Engine parameters	Specification
Engine model	DEUTZ F1L511
Number of cylinders	1
Bore, mm	100
Stroke, mm	105
Displacement, cc	824
Rated power, kW/hp	5.775/7.7
Rated speed, rpm	1500
Idle speed, RPM	900
Maximum torque, N.m	44/900 rpm
Injection point	24° C.A, bTDC
Type of injection	Direct injection
Type of cooling	Air cooling
Starting up	Electrical
Injection pressure	175 bar

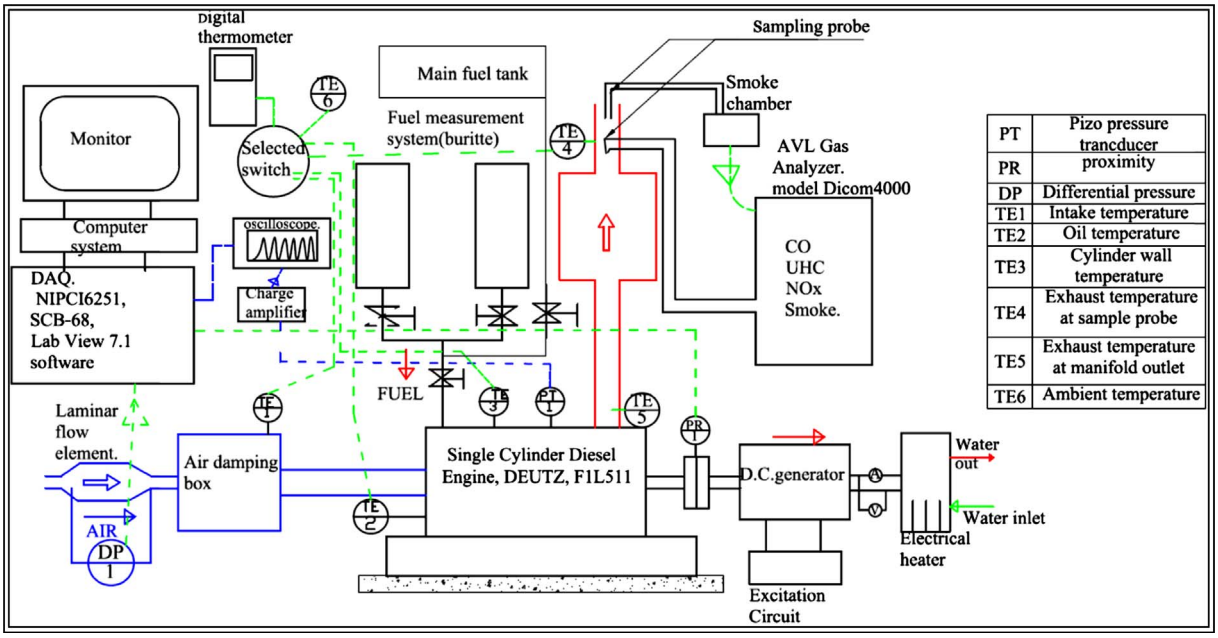

Fig. 1. The layout of the experimental test rig.

Table 2
Specification of the exhaust gas analyzer.

Gas emission	Measuring range	Resolution	Uncertainty
Smoke opacity	0–100%	0.1%	0.1%
CO	0–10% by vol.	0.01% by vol.	0.1%
CO_2	0–20% by vol.	0.1% by vol.	0.5%
UHC	0–20000 ppm	1 ppm	3%
O_2	0–25% by vol.	0.01% by vol.	0.04%
NO_x	0–5000 ppm	1 ppm	0.02%
Engine speed	250–8000 rpm	10 rpm	0.125%
Oil temperature	0–120 °C	1 °C	± 1 °C

The heat transfer calculations are not very sensitive to the wall temperature. The wall temperature (Tw) was experimentally estimated as 450 K, which yielded satisfactory results. There are many models for heat transfer coefficient (h_c). The most commonly employed for a diesel engine is Hohenberg Correlation [44].

$$h_c = C_1 \times V^{-0.06} \times p^{0.8} \times T^{0.4} \times (C_2 + V_m)^{0.8} \quad (5)$$

where p is the immediate pressure, in bar, C_1 and C_2 constant values are equal 130 and 1.4, respectively.

2.2. Ignition delay

The ignition delay is a significant parameter in a diesel engine combustion. It has a substantial impact on the combustion process, which will be reflected on performance and exhaust emissions of the engine. This period is counted from the start of fuel injection (SOI) into the combustion chamber to the point where the pressure-time curve separates from the motoring curve indicated as the start of combustion (SOC). The start of fuel injection can be defined by the engine design specification (injection needle lift at 24° bTDC for engine test rig). The start of combustion is harder to measure, but it can be estimated by the following approaches [45]:

- When the heat release rate becomes zero (that is when the cumulative heat release is at a minimum)
- The start of combustion can be defined as the minimum that occurs in the first derivative of cylinder pressure after the onset of injection.
- Can be defined by the start of combustion from pressure theta diagram, when the start of rapid pressure rise.

In the current study, two approaches for the time delay period have been tested to obtain the better of them. The ignition delay period estimated using the pressure rise rate is comparable to that achieved by using the heat release rate. Thus, the ignition delay period for the different fuel types and operating conditions is investigated using the pressure rise rate approach.

2.3. Mass fraction of burned fuel

One technique used in engine simulation modeling is to estimate the mass fraction burned as a function of engine crank angle using the Wiebe function [42]. The Wiebe function is expressed in Eq. (6) [46]. The Wiebe function has a characteristic S-shaped curve, and it is popularly utilized to characterize the combustion process. The mass fraction burned shape increases from zero, where zero mass fraction burn indicates the start of combustion, and then increases to unity showing the end of combustion. The variance between those two periods is known as the duration of combustion [46].

$$X_b(\theta) = 1 - \exp\left(-a \times \left(\frac{\theta - \theta_0}{\theta_d}\right)^{m+1}\right) \quad (6)$$

where X_b (θ) is the burned fuel fraction at the instantaneous crank angle, a is a constant for a combustion duration corresponding to 0–99.9% mass fuel burned, and it is equal to 6.908, θ_0 is the position of the crank at the beginning of the combustion, and it is also called the start of combustion (SOC), θ_d is the combustion duration, and m is a parameter that determines the speed of combustion and it can be calculated by the following equation [46]:

$$\tau_{\max} = \frac{\theta_{\max}}{\theta_d} = \left[\left(\frac{1}{6.908}\right) \times \left(\frac{m}{m+1}\right)\right]^{\frac{1}{m+1}} \quad (7)$$

where θ_{max} is the crank angle duration from the start of combustion to the position of Q_{gross} maximum.

The value of the parameter (m) is calculated from Eq. (7) for different fuel at an engine speed of 1500 rpm and various loads as shown in Table 3.

Table 3
Parameter (m) calculation for tested fuel at 1500 rpm for various loads.

Fuel type	Loads	Start of combustion	Theta at Q_{gross} maximum	θ_{max}	θ_d	m
D100	50%	−7	1.5	8.5	59	0.435
	75%	−7.5	−0.5	7	67.5	0.466
JB20D	50%	−6.5	1.5	8	59.5	0.4929
	75%	−7	0	7	71.5	0.4746
JB20D10A	50%	−6	1	7	58	0.459
	75%	−7	−0.5	6.5	69	0.4578
JB20D20A	50%	−7.5	1.5	9	59.5	0.4578
	75%	−8.5	−1.5	7	70.5	0.5027
JB20D30A	50%	−7	1.5	8.5	58.5	0.4653
	75%	−8	−1	7	68.5	0.4446
JB20D40A	50%	−7	1	8	60	0.5027
	75%	−7.5	−1	6.5	70.5	0.3645
JB20D50A	50%	−6.5	1	7.5	61.5	0.4644
	75%	−7	−0.5	6.5	70	0.3667

Quantitative evaluations of the expected uncertainty in the present measurements were estimated by using the procedure of Kline [47]. The peak uncertainty in the measurement of engine brake power, brake specific fuel consumption, and engine speed were found to be 0.9%, 2.2% and 0.15% (± 2 rpm), respectively.

First, the experimental test procedure discussed in the present work starts by warming up the engine using diesel fuel stored in the main tank. Next, the fuel line is switched to use the test fuel. Then, the specific engine load percentage is adjusted by regulating the excitation voltage supplied to the generator. After that, the rack location is used to control the required engine speed. Finally, the different readings from the measuring devices for a particular test are recorded at steady state condition of the engine operation. This procedure is repeated to cover the engine speed range at the specified load percentage; according to the test program summarized in Table 4. At the end of a specified load test, the engine is allowed to run using diesel fuel for half an hour, under no load at 900 rpm to avoid thermal cracking, and make sure that the engine fuel system is cleaned from any residuals of the previously tested fuel.

3. Jojoba methyl ester production

In the present work, the Egyptian raw Jojoba oil is utilized to produce the biodiesel fuel using a laboratory-scale setup. The manufacturer provided the technical specifications, and fatty acid composition of the Egyptian raw Jojoba oil are listed in Tables 5 and 6 [9]. The tools and devices used in the transesterification process are shown in Table 7 while the schematic diagram of JME preparation setup is illustrated in Fig. 2. The preparation process was conducted according to the conditions summarized in Table 8.

FT-IR spectrometry is a rapid and precise method for quantification of FAME. FT-IR spectrometry identifies the primary functional group's presence at both the optimum produced Jojoba biodiesel sample and its parent raw Jojoba oil [48]. Bruker-Spectrum Model Vertex 70 in a wavelength range of 400–4000 cm^{-1} was used to identify functional groups and the bands corresponding to different vibrations. The most characteristics absorption peaks of the raw Jojoba oil were indicated in Fig. 3(a). The absorption peak appearing at 719.61 is representative to $-CH_2$ rocking and the other one at 1738.91 is representative to C═O ester stretch. The FT-IR applied for Biodiesel produced using optimum conditions were nearly similar. Fig. 3(b) showed the produced biodiesel absorption peaks appearing at 1453.63 which is the methyl ester group ($CO-O-CH_3$) and the characterization peak at 1173.6 is due to (C—O) ester peak. It was evident the reduction of CH_2-O groups in raw oil and the appearance of CH_3-O- vibrations in Jojoba biodiesel. Also, the split of 1173.6 in the raw oil sample into 1179.75 and 1055.45 in the biodiesel sample indicates the conversion of raw oil into biodiesel. The main difference between the two FTIR spectrums is related to the transformation of ester groups at the raw Jojoba oil sample into methyl esters at the produced biodiesel [48]. The FT-IR spectrum is similar to that reported for Jojoba biodiesel oil by Shah et al. [49].

Gas Chromatography-Mass Spectrometry (GCMS-Model, QP2010Ultra, Shimadzu, Japan) fitted with 5MS column (30 m, 0.25 mm ID, 0.25 μm) was used to study the chemical composition of the Jojoba oil biodiesel product. The GC–MS of Jojoba biodiesel is shown in Fig. 4. There were five key feature peaks of fatty acid methyl esters (FAMEs) appearing by the retention time and the fragmentation pattern data of GC–MS analysis. These five peaks identified FAMEs as 9-Octadecenoic acid methyl ester (E) (peak 2), Oleyl Alcohol (peak 3), Cycloporopaneoctanoic acid 2-hexyl-methyl ester (peak 4), 1,19-Eicosadiene (peak 5) and 13-Docosenoic acid methyl ester (Z) (peak 7). The identified FAMEs were verified by retention time data and mass fragmentation pattern from previous studies [49].

4. Dispersion of AL_2O_3 nanoparticles with JB20D mixture

The Al_2O_3 nanoparticles were dispersed into a combination of Jojoba biodiesel-diesel fuel at the recommended composition (JB20D) with the aid of an ultrasonicator (Hielscher ultrasonic Model UP200S40) set at a frequency of 24 kHz for 30 min. The Alumina nanoparticles of the average size of 20–50 nm are supplied by Nanotech Egypt Company, with detailed specifications list in Table 9.

From Table 9, it can be observed that the thermal conductivity of Al_2O_3 at room temperature is over 30 times greater than that of JB20D blends. Thus, JB20D blends containing suspended Al_2O_3 are expected to exhibit significantly higher thermal conductivity relative to diesel-biodiesel blends. Therefore, the evaporation rate of fuel droplets will be increased, which in turn corroborates shorter ignition delay. Also, the surface-area-to-volume ratio of Al_2O_3 is higher than JB20D blends. Consequently, Al_2O_3-JB20D fuels predictably have superior heat transfer properties compared to JB20D blends.

The Manufacturer provides the transmission electron microscope (TEM) of alumina nanoparticles as shown in Fig. 5. TEM morphology of Al_2O_3 nanoparticles confined to the crystalline nature with minimal agglomeration and aggregate formation. The average grain structure was about 30 nm. X-ray Diffraction (XRD, Shimadzu X-lab 6100, Japan) of Al_2O_3 nanoparticles is shown in Fig. 6(a). The diffraction peaks of γ-Al_2O_3 with different planes confirm to the crystalline structure of nanoparticles. Sharp peak was observed at $2\theta = 25.26^\circ$ from which the grain size is calculated using Debye-Scherer's method, $D = (k * \lambda)/(\beta * \cos\theta)$ where D – average grain size of the nanoparticles, k – Shape factor (0.89), λ – X-ray wavelength of Al_2O_3 (1.54 Å), β – Full width at half maximum ($5.128 * 10^{-2}$), 2θ – Bragg angle (25.26°), $\theta = 12.36^\circ$ and hence, D is calculated to be 27.36 nm. The X-ray Diffraction analysis is similar to that reported for Al_2O_3 nanoparticles by Venu et al. [40].

The Al_2O_3 nanoparticles were analyzed by Fourier transform infrared (FT-IR), using a Bruker-Spectrum Model Vertex 70 in a wavelength range of 400–4000 cm^{-1} to identify functional groups and the

Table 4
The experimental program.

Fuel type	Load percentage	Speed
D100 JB20D JB20D10A JB20D20A JB20D30A JB20D40A JB20D50A	No load, 25%, 50%, and 75%	900, 1100, 1300, 1500 and 1700 rpm

Table 5
Specifications of the utilized raw Jojoba oil [9].

Property	Range
Freezing point	10.6–7.0 °C
Melting points	6.8–7.0 °C
Boiling point	398 °C
Flash point	295 °C
Specific gravity at 25°	0.863
Viscosity	
100 °C	57.9 mm^2/s
25 °C	27 mm^2/s
Viscosity index	232
Iodine value	82 mg KOH/g oil
Average molecular weight of wax esters	606 kg/kmol

Table 6
The fatty acid composition of raw Jojoba oil [9].

Fatty acid	Relative percentage %
Oleic (C18:1)	2.47
Linoleic (C18:2)	0.38
Eicosenoic (C20:1)	46.8
Erucic (C22:1)	39.8
Tricosanoic (C23:0)	2.09
Lignoceric (C24:0)	6.27
Nervonic (C24:1)	2.16

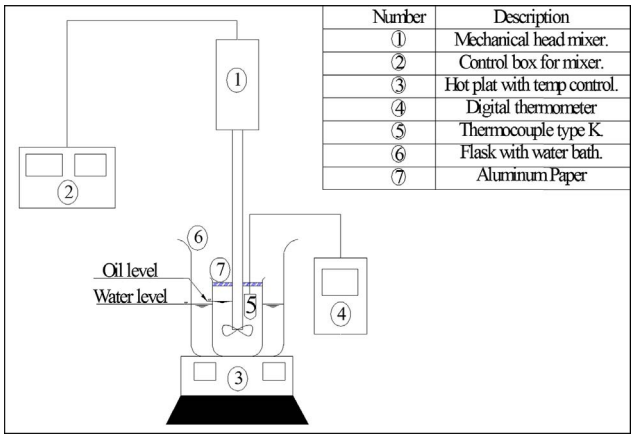

Fig. 2. Schematic diagram of JME preparation setup.

Table 8
Optimum condition of the transesterification process.

Catalyst and concentration	Methanol: oil molar ratio	Reaction time, h	Reaction temperature, °C	Mixing intensity, rpm	Washing times
KOH, 0.5 wt%	6:1	2	60 ± 1	600	4–5

bands corresponding to different vibrations as shown in Fig. 6(b). From this figure, it can be observed that the high broadband at 3600–2500 cm^{-1} occurring for the γ-Al_2O_3 is due to various −OH groups at the surface. The bands below 1150 cm^{-1} correspond to Al−O vibrations. The band at 1632 cm^{-1} represents the scissoring vibrations of two O−H bonds in physisorbed water molecules or can be connected to the small amount of adsorbed impurities (such as CO_2 or carbonates) [50]. The FT-IR analysis is similar to that reported for γ-AL_2O_3 nanoparticles by Ledwa et al. [51].

The AL_2O_3 nanoparticles are weighted regarding the predefined mass fraction in the range of 10–50 mg/l with the step of 10 mg. Correspondingly, the received mixture is symbolized as JB20D10A, JB20D20A, JB20D30A, JB20D40A, and JB20D50A indicating Alumina nanoparticle contents of 10, 20, 30, 40, and 50 mg/l into the JB20D mixture, respectively. A sample of JB20D containing 50 mg/l Al_2O_3 was kept in a long tube under static conditions to observe mixture stability. There was no mixture settling recorded for about one week.

The properties of the pure diesel fuel, JME, JB20D without and with Al_2O_3 were measured according to ASTM standards, as listed in Table 10. The most critical fuel properties that affect engine performance are the viscosity, heating value, and cetane number. Viscosity is an important characteristic, as it affects fuel atomization and operation of the fuel injection system. Fuel atomization improves as fuel viscosity decreases. Regarding the properties of fuels, the JB20D blend has a higher viscosity and molecular weight over those of diesel fuel by about 22% and 18%, respectively, while the addition of Al_2O_3 nanoparticles into the JB20D blend increases the kinematic viscosity by about 8%. The heating value for the JB20D blend is decreased slightly as compared to diesel fuel, while the heating value is approximately the same with the addition of Al_2O_3 nanoparticles into the JB20D blend. The self-ignition temperature of the fuel is a critical ignition quality parameter. Lower self-ignition temperature resulted in a shortened ignition delay period. Cetane number is used for comparing the ignition quality of fuels. The ignition delay decreases with the increase in cetane number with all the other parameters affecting ignition quality being the same. The cetane number is increased by about 5% for JB20D blend compared to diesel fuel, while the cetane number is enhanced by about 10% due to the addition of Al_2O_3 nanoparticles to JB20D blend. Oxygen content improves the combustion quality of fuel. On contrast, it decreases fuel heating value. The oxygen content in Jojoba biodiesel is about 13% by mass. These properties affect and govern the combustion behavior of JB20D as an alternative fuel in the diesel engine. Test results have also shown positive effects on the combustion process with the addition of Al_2O_3 to JB20D blend.

5. Results and discussions

The thermal analysis, mechanical performance and the emission characteristics of a diesel engine using diesel oil and JB20D blend with and without Al_2O_3 nanoparticle additives regarding test program in

Table 7
Summary of the used devices in the transesterification process.

Device	Specifications
Mechanical stirrer (Servodyne mixer head model 50003–45 with mixer controller model 50003–05)	Speed from 150 to 6000 rpm with a resolution of 1 rpm, Maximum torque is 1.2 kg.cm Counter downtime up to 99 min., 59 s with time accuracy of ± 1 s. Dimensions (L × D) are (292 × 92 mm)
Temperature controllable digital and ceramic hot plate (Start Scientific Model SM26)	Temperature range (25–300 °C) Temperature resolution 0.1 °C
Glass beakers	50 ml, 250 ml, 500 ml, 2000 ml
Sensitive scale, Denver instrument company, model AC-12 k.	Capacity 1200 g, Sensitivity 0.1 g, Automatic calibration, Pan size 20 * 23 cm
Type K thermocouple	Omega with accuracy ± 2 °C
Temperature thermometer EXTECH Model AZ-8852	Range (−200 to 1370 °C), Accuracy (± 0.1% rdg + 0.7 °C), Resolution 1 °C

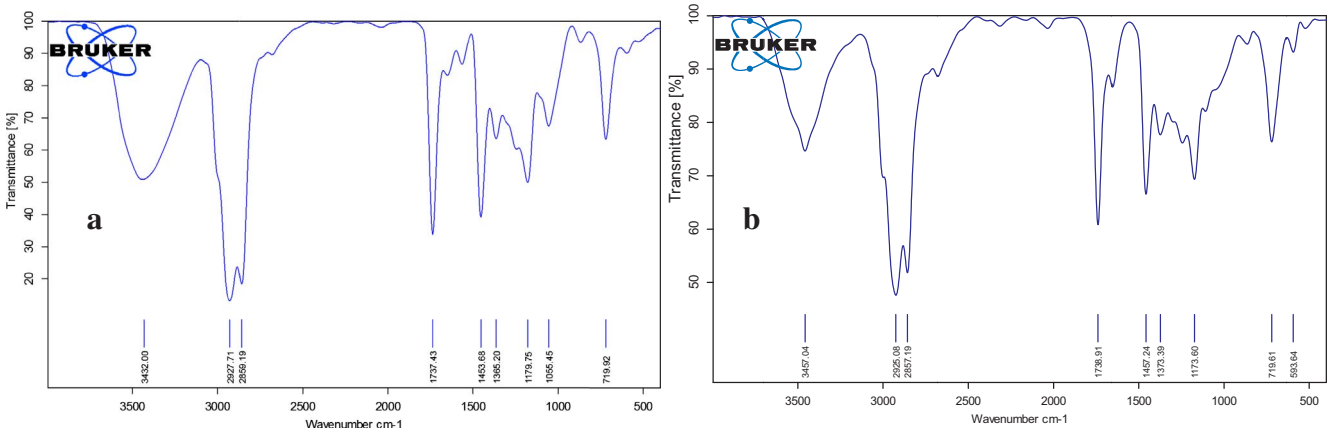

Fig. 3. FT-IR spectrum for (a) raw Jojoba oil (b) Jojoba biodiesel oil.

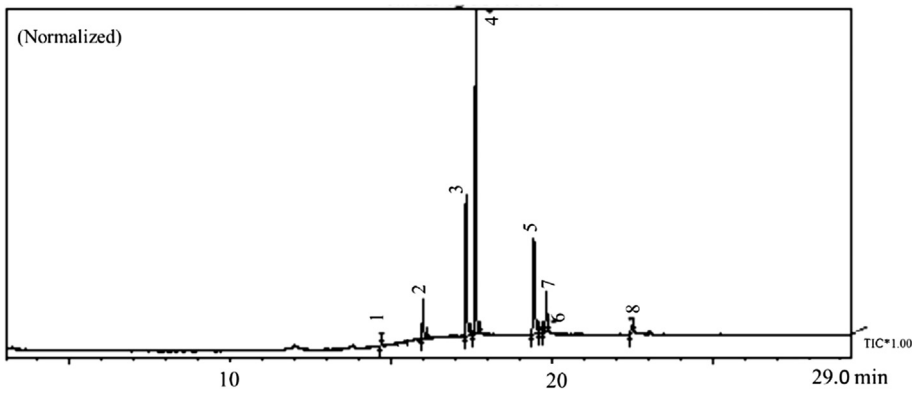

Fig. 4. Gas chromatography–mass spectrometry of Jojoba biodiesel.

Table 9
Details of alumina nanoparticles.

Item	Specification
Manufacturer	Nanotech Company, Egypt
Chemical name	Gamma Aluminum Oxide (Alumina, Al_2O_3) Nano powder, gamma phase, 99.9%
Average particle size	20–50 nm
Surface area (SSA)	> 150 m^2/g
Appearance	White
Thermal Conductivity	~35 W/m.K
Melting point	2045 °C
Boiling point	2980 °C
Density	3.9 g/cm^3

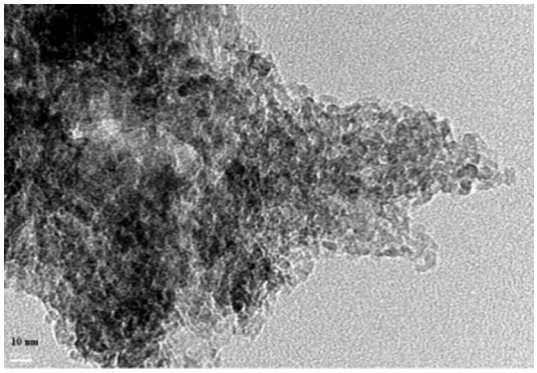

Fig. 5. TEM image of Al_2O_3.

Table 4 were determined. Based on the combustion data, cylinder pressure, pressure rise rate, gross heat release rate and mass fraction of burned fuel were plotted against the crank angle, while the ignition delay period was plotted against engine load percentage. The performance parameters, such as brake specific fuel consumption and exhaust gas temperature as well as the emission concentrations of NO_x, CO, UHC and smoke opacity were plotted against the engine speed.

5.1. Combustion characteristics

5.1.1. Cylinder pressure

Fig. 7 shows the change of cylinder pressure for tested fuels with various speeds at 75% load. Using the JB20D blend led to a lower value of peak pressure (by about 1.5%), and its location is retarded when compared to diesel fuel. This is attributed to the adverse effect of its higher viscosity and molecular weight which lead to inefficient utilization of fuel energy contents [15]. However, the retardation to receive this peak value could be attributed to the increase in the ignition delay period necessary to balance the effect of the high viscosity of fuel burned that worsen the processes of fuel atomization and evaporation. These results have a good agreement with findings that were obtained by Shehata and Abdel-Razek [15].

The beginning of the combustion process is remarkably advanced with the addition of Al_2O_3 into the JB20D mixture. Also, the peak pressure was increased with the addition of nanoparticles for all engine speeds. This is attributed to the higher surface to volume ratio and thermal conductivity of Al_2O_3 nanoparticles which improved the evaporation rate of the fuel droplets, resulting in enhanced combustion process. The maximum peak pressure was obtained at the dose level of 30–40 mg/l for all engine speeds. These results have a good agreement with that cited in the literature [40,52].

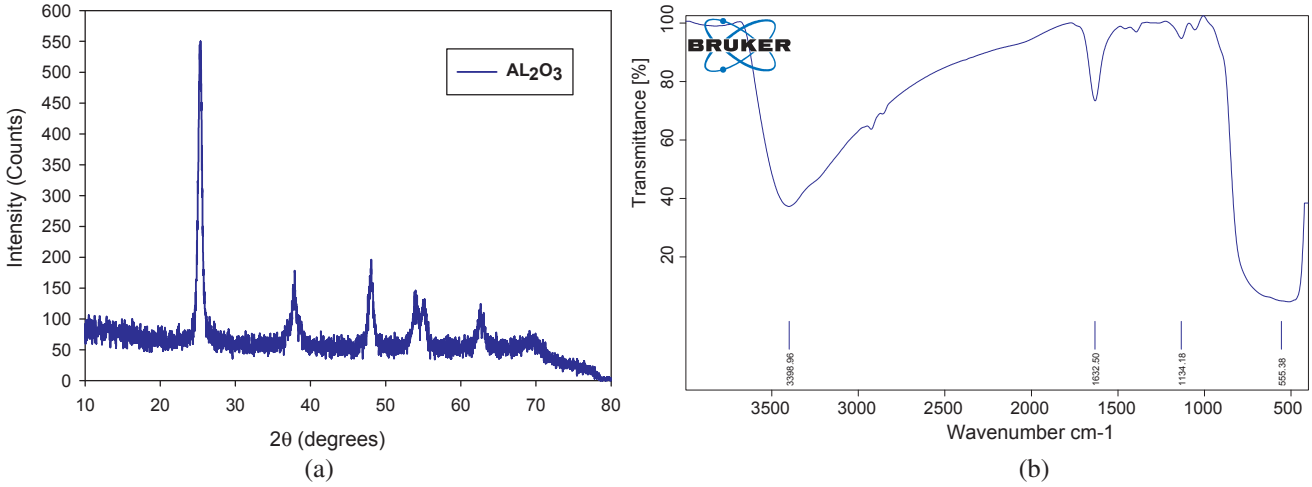

Fig. 6. Al_2O_3 nanoparticles (a) XRD, (b) FT-IR spectrum.

It is essential to record the peak pressure and its location relative to the crank angle. These factors were recorded for all runs to get a real indication of how fast the heat liberation rate is finished against the upward piston motion. Fig. 8, represent the peak pressure and its location with the different operating conditions and various tested fuels. At lower engine speed the cylinder aerodynamics is worsened, and it is necessary to inject a relatively higher fuel volume to compensate the weak mixing effect between fuel and air. Thus, the peak pressure may be increased while its position is retarded. Also, the results presented in this figure reveals that the position of where the maximum cylinder pressure is attained for the tested fuels have the same trends with the engine speed but with different numerical values. However, for JB20D blended fuel, this position is retarded in comparison with that for D100, due to the high viscosity effect. Also, for all the tested fuels, the position of P_{max} decreases with the increase in engine speed due to mixing and combustion process improvements because of higher turbulence intensities. As the engine speed increases, the delay period decreases, start of combustion is advanced and P_{max} occurs earlier. These results have a good agreement with Shehata and Abdel-Razek [15]. At high load and high speed, the peak pressure is decreased, which could be due to the increase in friction losses resulting in reduced heat release rate. The addition of Al_2O_3 additives into JB20D blended fuel leads to an advanced position of P_{max}. This is attributed to improved evaporation rate and better fuel-air mixing resulting in shortened ignition delay. The maximum advance in the position of peak pressure occurs at Al_2O_3 additives dose level of 20–30 mg/l. Furthermore, the maximum value of the percentage increase of the cylinder pressure is about 4.5% at Al_2O_3 additives concentration of 30–40 mg/l as compared to JB20D mixture fuel. These results were comparable with that obtained by Selvan et al. [28] and Sajith et al. [30].

5.1.2. Pressure rise rate

The shape of the pressure rise rate curve depends on whether the combustion process is fast or weak. Under normal conditions, the position of peak pressure rise rate occurs after TDC but not too far [42,45]. The point of attainment the peak pressure rise rate indicates that the major part of the heat release due to premixed combustion mode has taken place. This peak of pressure rise rate is followed by a sharp fall in the rate of pressure rise and a steady value of dp/dθ [45]. The rate of pressure rise is a direct indication of the rate at which the heat is released, and thus the degree to which the reaction proceeds. The maximum value of pressure rise rate is an important design parameter reflecting the dynamic limits to be withstood by different engines components [40]. The rate of pressure rise is the differential of the cylinder pressure data with respect to the crank angle (θ).

Fig. 9 represents the variation of pressure rise rate with the crank angle when the engine is fueled by diesel fuel, JB20D with and without Al_2O_3 additives at 75% load and different engine speeds. The results showed that the maximum rate of pressure rise rate for JB20D is slightly lower than that for diesel oil. This is attributed to the laminar burning velocity for JME is found to be lower than that for diesel fuel [12], which leads to a decrease in heat release rate and consequently reduce the pressure rise rate. These results have a good agreement with Radwan et al. [12]. The addition of Al_2O_3 nanoparticles into JB20D fuel blend leads to an increase of fuel droplet evaporation rate and better fuel-air mixing. Thus, the overall combustion process improved leading to higher peak pressure rise rate as compared to the JB20D mixture. This effect could be attributed to the catalytic behavior of Al_2O_3 nanoparticles during the combustion process resulting in higher cylinder pressure as well as higher rate of pressure rise.

Table 10
Properties of diesel oil, JME, JB20D without and with Al_2O_3 samples.

Property	Testing method	Diesel oil	JME (B100)	JB20D	JB20D10A	JB20D20A	JB20D30A	JB20D40A	JB20D50A
Calorific value, kJ/kg	ASTM D-240	45448	44866	45432	45439	45445	45453	454563	45467
Viscosity @40 °C, mm^2/s	ASTM D-445	3.34	11.72	4.06	4.12	4.28	4.29	4.32	4.38
Molecular weight, kg/kmol	–	191.02	350.73	223.96	–	–	–	–	–
Specific gravity at 15.56 °C	ASTM D-1298	0.8421	0.8645	0.8471	0.8471	0.8471	0.8471	0.8471	0.8471
Cetane index	ASTM D-976	49.5	–	52	53.1	54.4	55.2	56.6	57
Initial boiling point, °C	ASTM D-86	180	185	180	–	–	–	–	200
Elemental analysis, % by mass									
C%		86.21	76.01	–	–	–	–	–	–
H%		11.59	10.05	–	–	–	–	–	–
N%		1.91	Nil	–	–	–	–	–	–
O_2%		Nil	13.64	–	–	–	–	–	–
S%		0.29	0.3	–	–	–	–	–	–

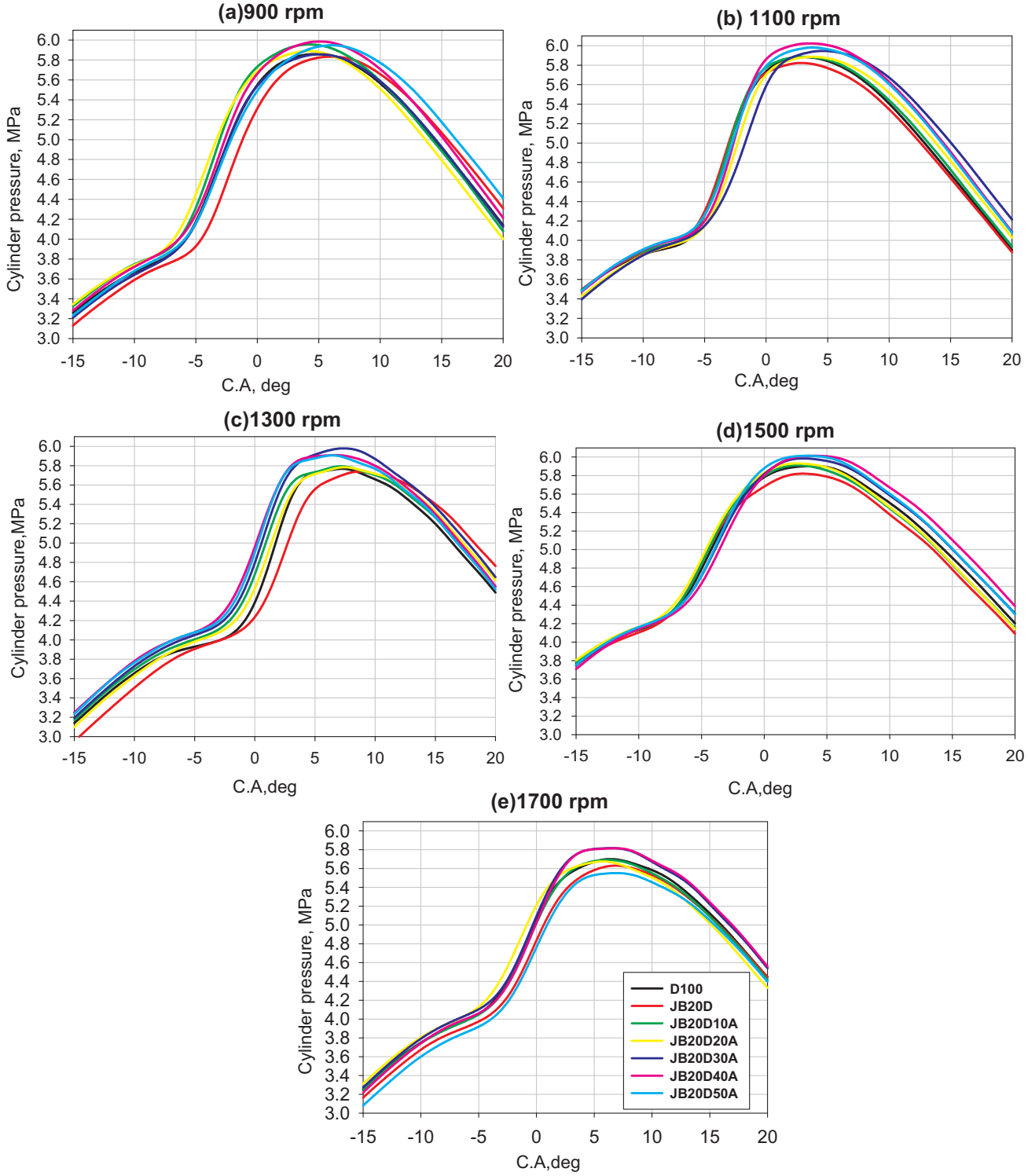

Fig. 7. The change of cylinder pressure with crank angle at different engine speeds and 75% load.

5.1.3. Gross heat release rate

The variation of gross heat release rate (dQg/dθ) as a function of crank angle for engine fueled with pure diesel fuel, JB20D with and without Al_2O_3 additives at 75% load with all engine speeds is shown in Fig. 10. The results showed that the heat release rate is negative during the ignition delay period [40]. This is mainly attributed to the cooling effect caused by fuel vaporization and heat losses to the engine cylinder walls. The peak gross heat release rate for JB20D is slightly lower as compared to those of diesel fuel. This is attributed to the higher molecular weight value and the lower laminar burning velocity of JB20D blended fuel as compared to those of diesel fuel [16]. At the engine speed of 1700 rpm, the gross heat release rate is slightly decreased, possibly due to increase in the friction losses. The gross heat release rate is higher for the Alumina nanoparticles blended JB20D fuels compared to pure JB20D blend. This could be attributed to the enhanced effect of surface area to volume ratio and the improved ignition properties of Alumina nanoparticles which initiate early start of combustion, leading to increased peak gross heat release rate compared

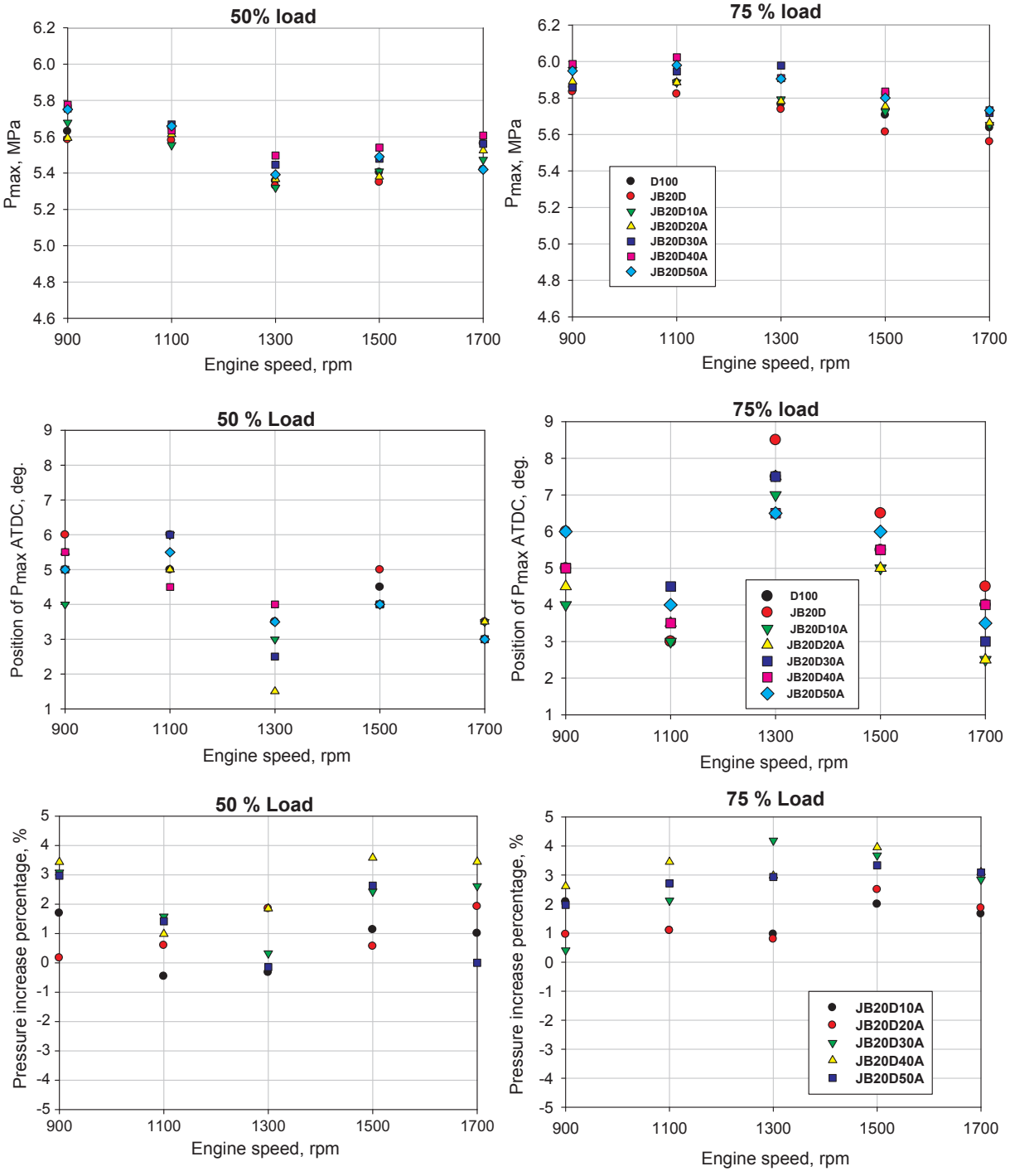

Fig. 8. The peak pressure and its position and the percentage increase of the cylinder pressure for different tested fuels at all engine speeds.

to JB20D blended fuel. These results have a good agreement with the literature [28,30,33,40].

5.1.4. Ignition delay period

The ignition delay period in the diesel engine has a significant influence on engine design and performance [53]. The ignition delay can be divided into two parts, physical delay and chemical delay [53]. It depends mainly on fuel properties and engine operating conditions in conjunction with fuel injection system features. Fig. 11 shows that the variation of ignition delay with engine loads for all tested fuel. Generally, for all engine speeds, it can be observed that the ignition delay is decreased with the engine load. This is attributed to an increase of the cylinder temperature and the turbulence intensity which in turn improve the fuel-air mixing and increase the fuel vaporization rate. These results have a good agreement with the literature [33]. The ignition delay for JB20D mixture fuel is slightly higher by about 0.5 CA as compared to diesel fuel. This is attributed to the higher viscosity and molecular weight of JB20D, which lead to an increase of fuel droplet size and vaporization time. The addition of Al_2O_3 nanoparticle leads to a decrease the ignition delay. The reason is attributed to the higher surface area to volume ratio and higher thermal conductivity of the Al_2O_3 nanoparticles which enhanced the evaporation rate, resulting in a reduction in physical delay. These results were confirmed with others cited in the literature [33,40].

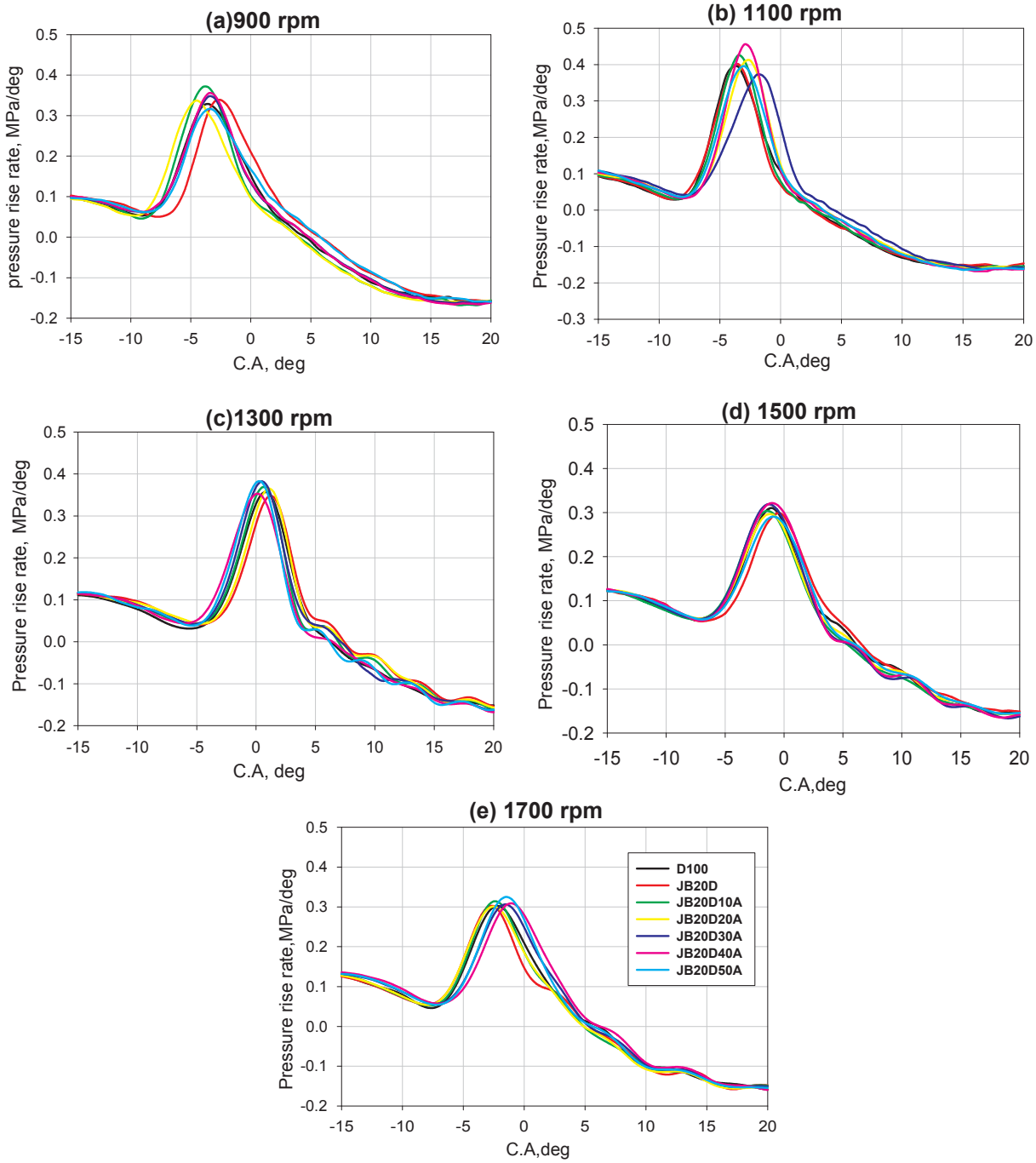

Fig. 9. Variation of pressure rise rate with crank angle at 75% load with different engine speeds for tested fuels.

5.1.5. Mass fraction of burned fuel

Mass fraction burned is the fraction of injected fuel burned and relative to the whole mass of fuel injected per cycle during the combustion process [42]. When combustion of the fuel-air mixture in diesel engine begins, a single flame front travels through the instantaneously injected fuel until it gets thoroughly burned. During the burning of the fuel, the combustion zone can be divided into burned and unburned zone. As the combustion proceeds, the burned region part is increased, and unburned zone portion is decreased. The variation in the mass fraction of burned fuel with a crank angle (CA) for diesel fuel, JB20D blend without and with Al_2O_3 additives at an engine speed of 1500 rpm with 50% and 75% load is shown in Fig. 12. It can be observed that 90% of the mass fraction of burned fuel for diesel fuel is burned faster than that for JB20D blended fuel. This trend may be attributed to the higher viscosity of JB20D that leads to delay at the beginning of combustion process. The addition of Al_2O_3 nanoparticles into JB20D blended fuel accelerated the start of combustion and reduced the combustion duration. This is attributed to the positive effect of the additives which increased the evaporation rate and improved the mixing of fuel with air, resulting in a reduction of the ignition delay. The minimum combustion duration was obtained at the Al_2O_3 nanoparticles concentration of 20–40 mg/l.

5.2. Engine mechanical performance

Fig. 13 shows the variation of bsfc and engine thermal efficiency at engine loads of 50% and 75% for different engine speeds. Using JB20D blend led to an increase in the bsfc by about 12% as compared to diesel

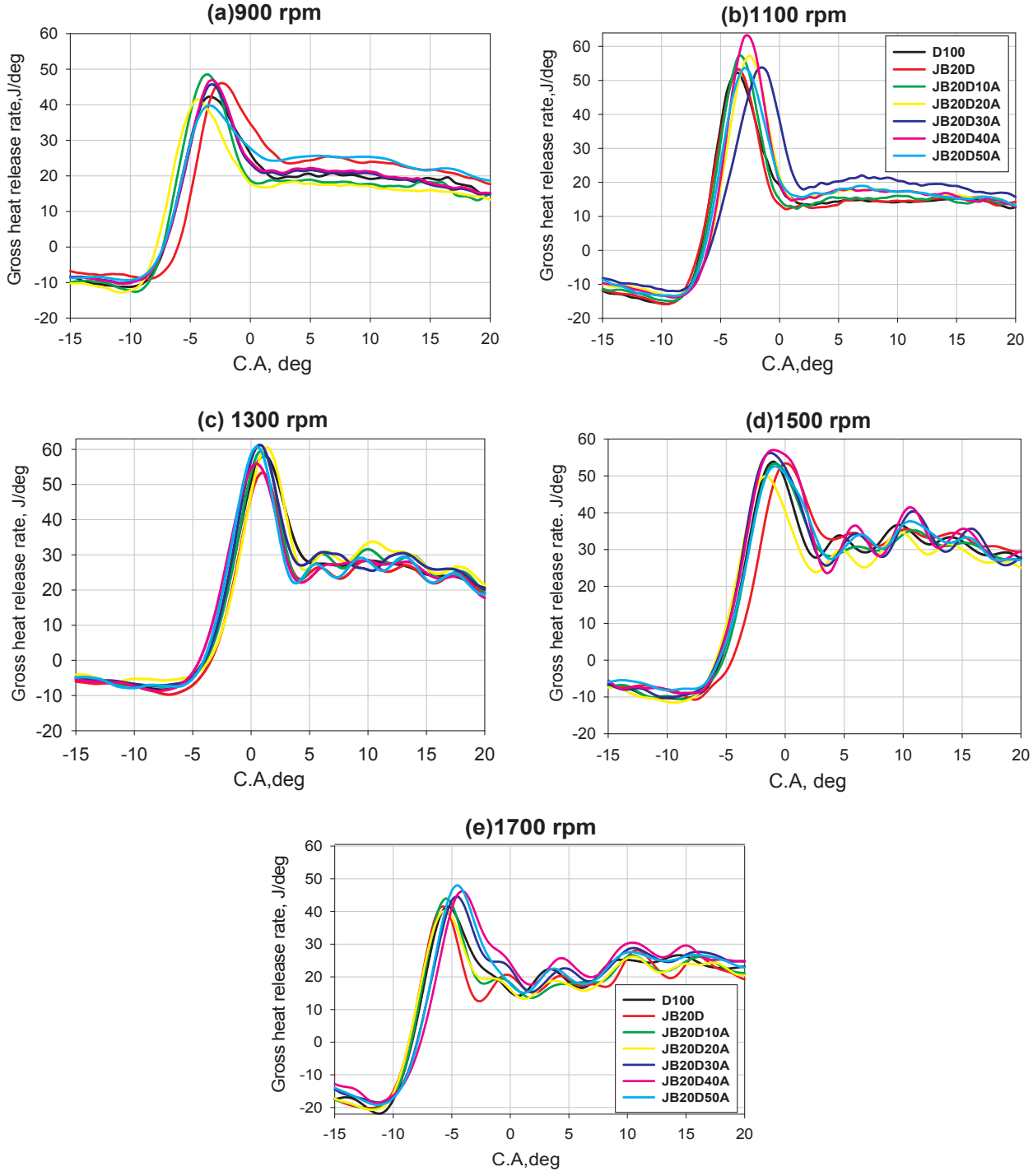

Fig. 10. Variation of gross heat release rate with crank angle at 75% load with different speeds for all tested fuels.

fuel, irrespective of the operating conditions. The main parameters that affect the bsfc are the fuel heating value and the combustion quality or the utilization of the fuel energy [45]. In this regard, the effect of the heating value is insignificant compared to that other effects. Therefore, the main parameters that affect the bsfc are parameters that control the combustion quality of the fuel. These parameters include the fuel viscosity and molecular weight. As discussed in the previous sections, the higher viscosity of JB20D leads to poor fuel atomization which in turn increases the amount of fuel burned in the diffusion mode which is characterized by lower combustion efficiency. From the molecular weight point of view, the fuel that has higher molecular weight needs more time and energy for the fuel degradation process, and consequently increasing in the ignition delay period. These results have a good agreement with the findings of Shehata and Abd-Elrazik [15].

From Fig. 13, it can be observed that the bsfc was decreased by 12% with the addition of Al_2O_3 nanoparticles. This improvement in the engine performance continues until the minimum bsfc which is achieved at the dose levels of 30–40 mg/l. At these concentrations, the bsfc is improved, to slightly lower than that of diesel fuel. Beyond these dose levels, the additional of Al_2O_3 nanoparticles leads to an increase again in the bsfc. This influence can probably be noticed from the improved cylinder pressure characteristics discussed in Section 5.1.1. The addition of nanoparticles improved the carbon oxidation rate in the combustion process, leading to complete combustion and reduction in

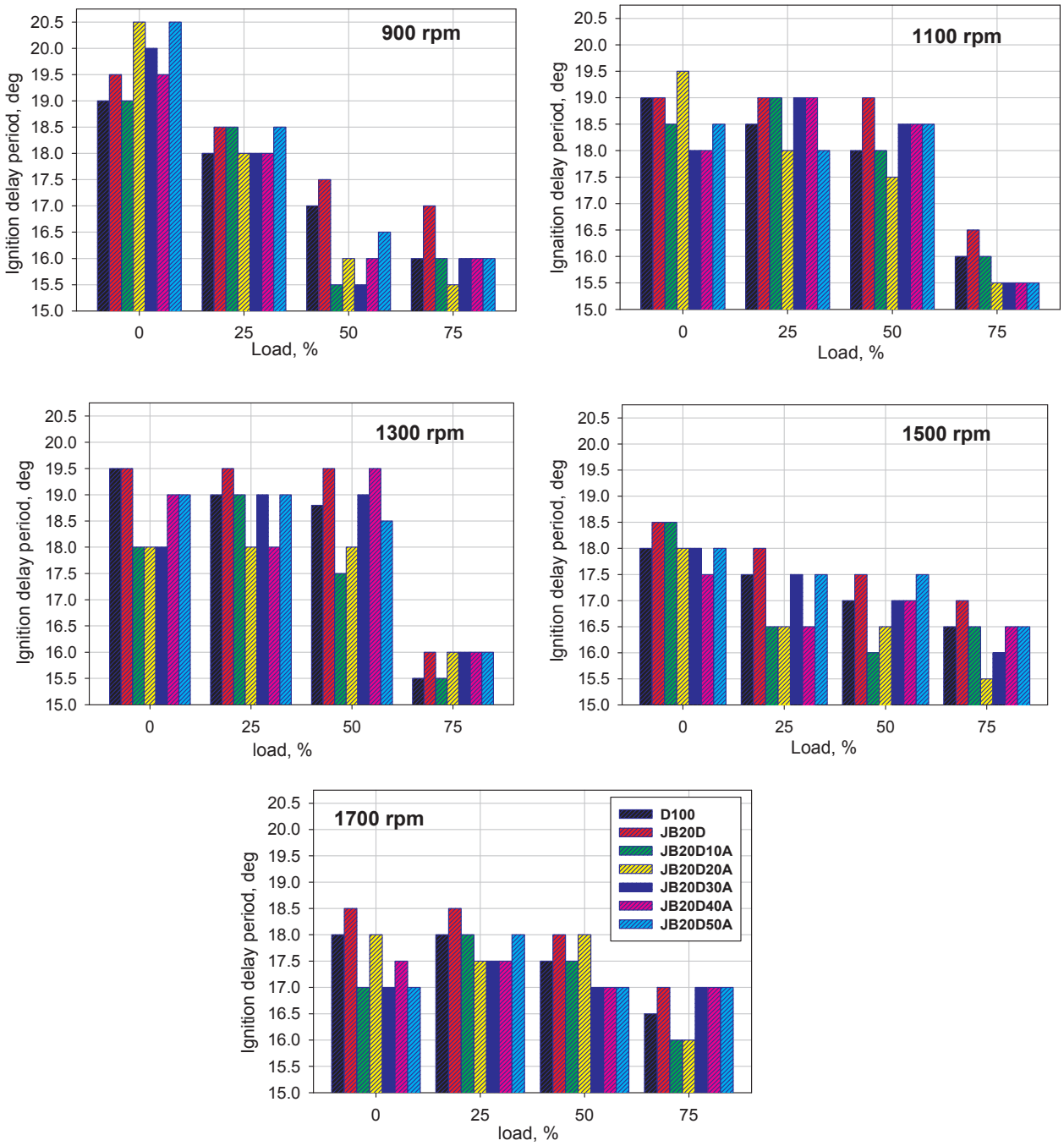

Fig. 11. The ignition delay period for tested fuel at different engine loads and speeds conditions.

the fuel consumption. These results have a good agreement with findings that were obtained by Ganesh and Gowrishankar [54], and Basha and Anand [34].

The variation of EGT with engine loads and speeds when using diesel fuel, JB20D without and with the addition of Al_2O_3 nanoparticles is shown in Fig. 14. Using of JB20D led to a lower value of EGT than those recorded when diesel fuel is used. This could be attributed to slower combustion resulting from the relatively poor combustion characteristics of the JB20D blended fuel. The addition of Al_2O_3 nanoparticles into JB20D reduced the exhaust gas temperature as shown in Fig. 15, irrespective of the operating conditions. This reduction in the EGT with increase of concentration level proceeds until certain dose; then EGT begins to rise again. The addition of Al_2O_3 nanoparticles decreased the bsfc as discussed above, and consequently reduced the energy content which in turn reduced the global exhaust gas temperature. Moreover, the results show that the addition of Al_2O_3 nanoparticles significantly improved the cylinder combustion process as discussed in Section 5.1.1. Thus, the required amount of fuel to produce the designated engine load at particular engine speed is reduced, which decreases the bsfc as presented in Fig. 13. Correspondingly, the energy content of the engine cylinder is reduced, and thus the global temperature of exhaust gases is reduced. Another reason may be that the addition of Al_2O_3 reduces the rich mixture zone in diffusion mechanism leading to lower exhaust gas temperature [31,55].

5.3. Engine emission characteristics

Fig. 15 shows the variation of engine emissions with engine speeds

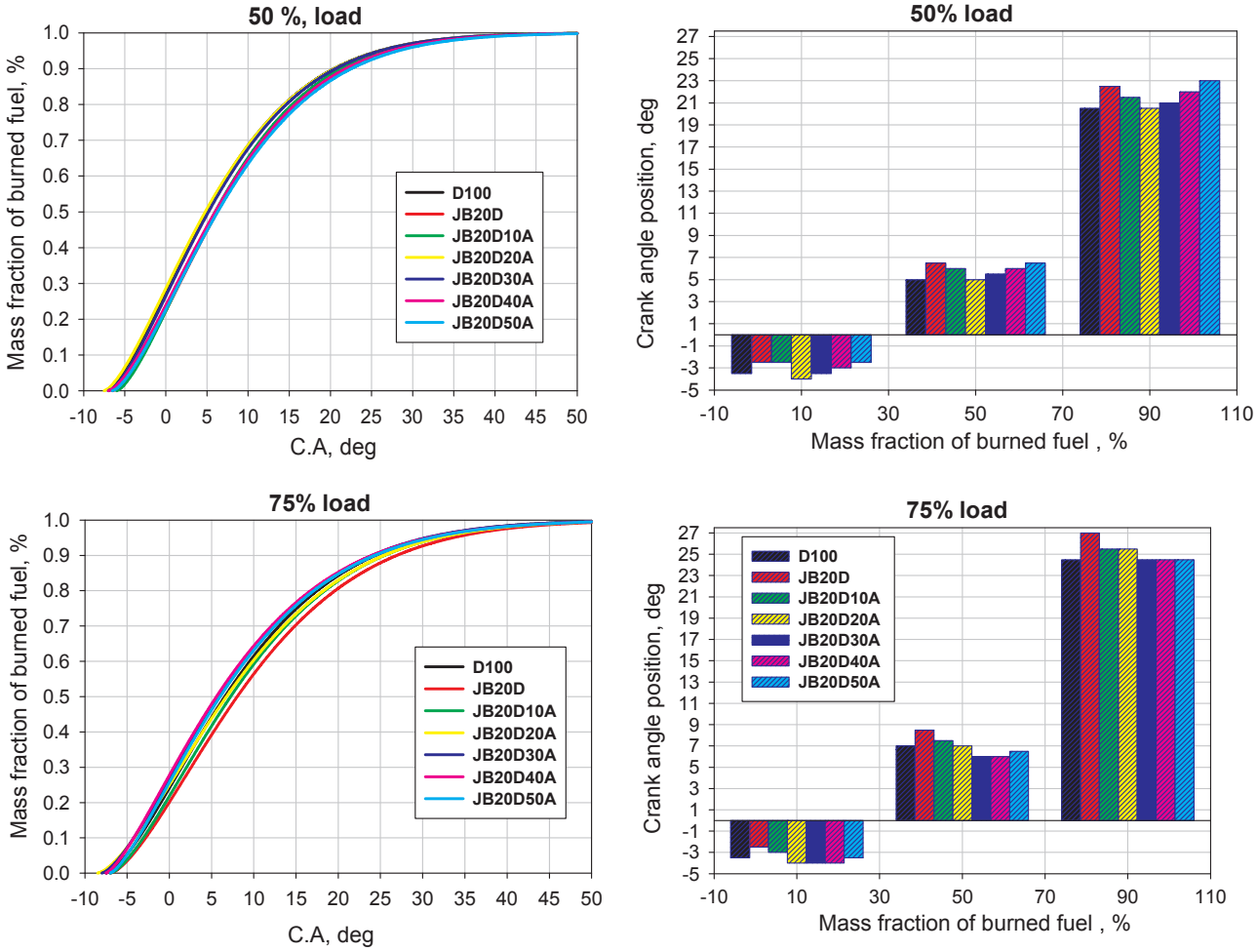

Fig. 12. The mass fraction of burned fuel and its position for 10%, 50% and 90% for tested fuel at 1500 rpm with different loads.

at 50% and 75% load when the engine is fueled by diesel fuel, JB20D without and with Al_2O_3 additives. At low engine speeds, the use of JB20D blend resulted in a considerable reduction in the NO_x emissions compared to diesel. This is mainly attributed to a decrease in the local reaction temperature. In contrast, at high engine speeds, this trend is opposite where it may be attributed to the increase of oxygen content in JME (contains 13% O_2), and thus the growth in the reaction temperature leading to an increase in NO_x emissions (Zeldovich mechanism). These results have a good agreement with findings of Al-Widyan et al. [18] and Shehata and Abdel Razek [15].

From Fig. 15, it can be observed that the NO_x emission was significantly reduced with the addition of Al_2O_3 nanoparticles as compared to the values for both diesel and JB20D blended fuels, irrespective of the engine conditions. This effect is attributed to the catalytic behavior of Al_2O_3 nanoparticles that facilitates the reaction to be completed forming the final products (heterogeneous combustion) with a minimum thermal breakdown of the hydrocarbon compounds. Therefore, the existence of lower active radicals lowers the possibility to form thermal NO_x. This catalytic behavior is decreased as the engine load is increased with the rise in-cylinder temperature, and thus the existence of greater chance of thermal NO_x formation. Furthermore, at high engine speeds the effect of nanoparticles on NO_x emissions is

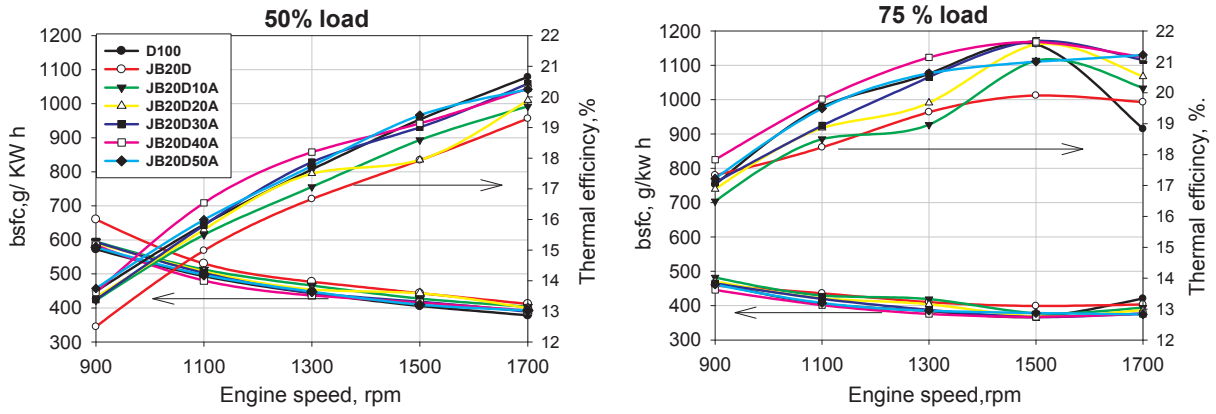

Fig. 13. The variation of the engine thermal efficiency and the bsfc with engine speeds at different loads.

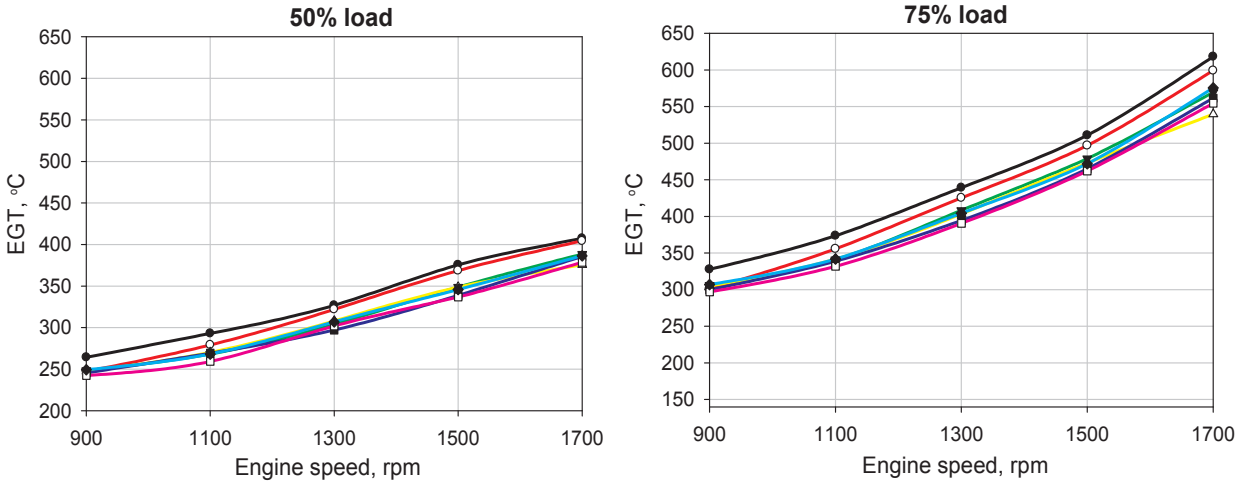

Fig. 14. Variation of EGT with engine speeds and loads using different fuel.

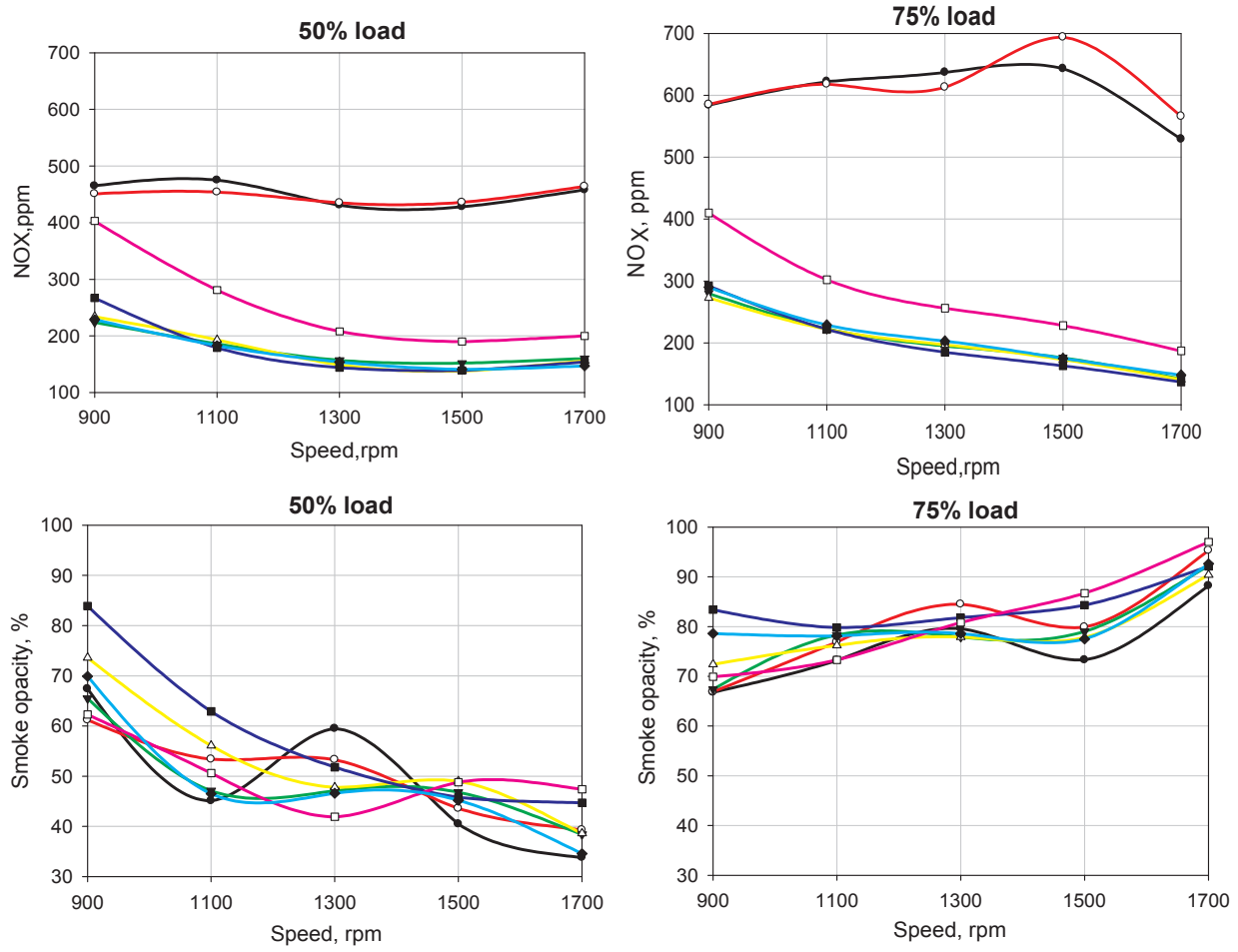

Fig. 15. Engine NO_x and Smoke opacity emissions with different loads and speeds.

approximately saturated, especially at low and half load conditions. As shown, there were slight differences in NO_x emissions regarding the dose level of nanoparticles in the fuel blend. This effect may be depending on the degree of combustion quality indicated by the peak pressure value. Correspondingly, the minimum NO_x emission was obtained at Al_2O_3 additives of 20–30 mg/L for all loads and speeds. These results were confirmed with findings that achieved by Ganesh and Gowrishankar [54] and Selvan et al. [28].

The variation of smoke opacity for tested fuel with different engine speeds and loads is shown in Fig. 15. At half load, for all tested fuels, the smoke emission was reduced with an increase in engine speed. In contrast, the smoke concentration increased as the engine speed increases at 75% load. This is attributed to insufficient oxygen to completely burn larger amounts of fuel, leading to reduced oxidation rate of carbon monoxide to CO_2, and thus higher concentrations of soot. Using JB20D fuel blend increased smoke emissions as compared to pure diesel fuel. This behavior is attributed to the lower chance of soot oxidation during the expansion stroke because of lower time for combustion

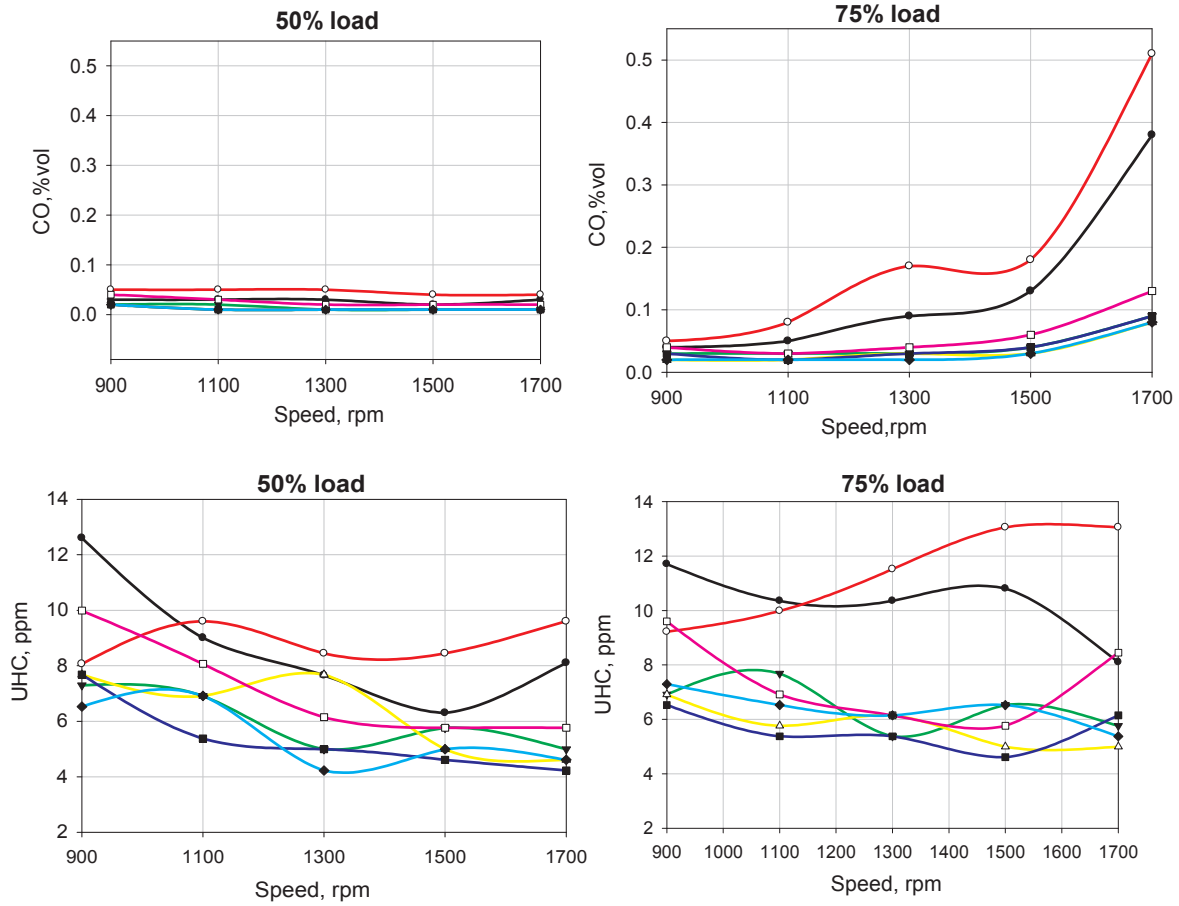

Fig. 16. Engine CO and UHC emissions with different loads and speeds.

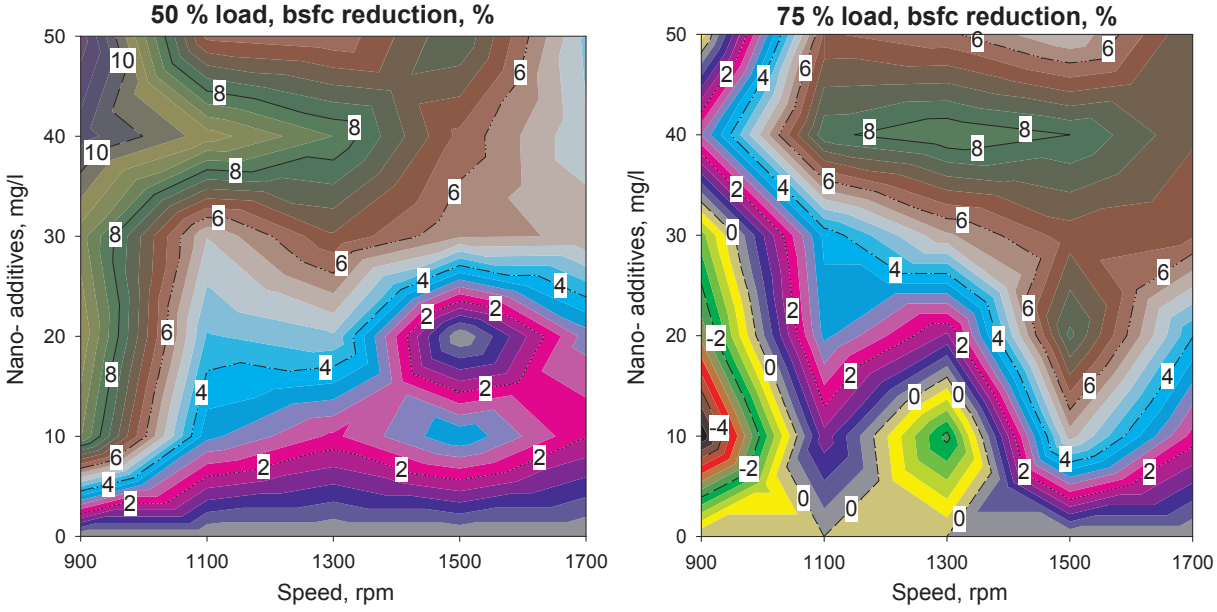

Fig. 17. The percentage reduction of bsfc at all engine loads and speeds conditions.

process and poorer fuel atomization, resulting in prolonged ignition delay.

The addition of Al_2O_3 led to a reduction in the concentration of smoke opacity as compared to JB20D blend as represented in Fig. 15. The reason is attributed to increased evaporation rate and improved fuel-air mixing resulting in shortened ignition delay and enhanced oxidation rate. Kao et al. [31] and Basha with Anand [33] also found similar trends of smoke reduction using Aluminum nanoparticles blended with biodiesel fuel.

The variation of CO and UHC emissions for tested fuels with engine speeds at various loads are presented in Fig. 16. At half engine loads, for all tested fuels the concentration of CO emission was relatively low

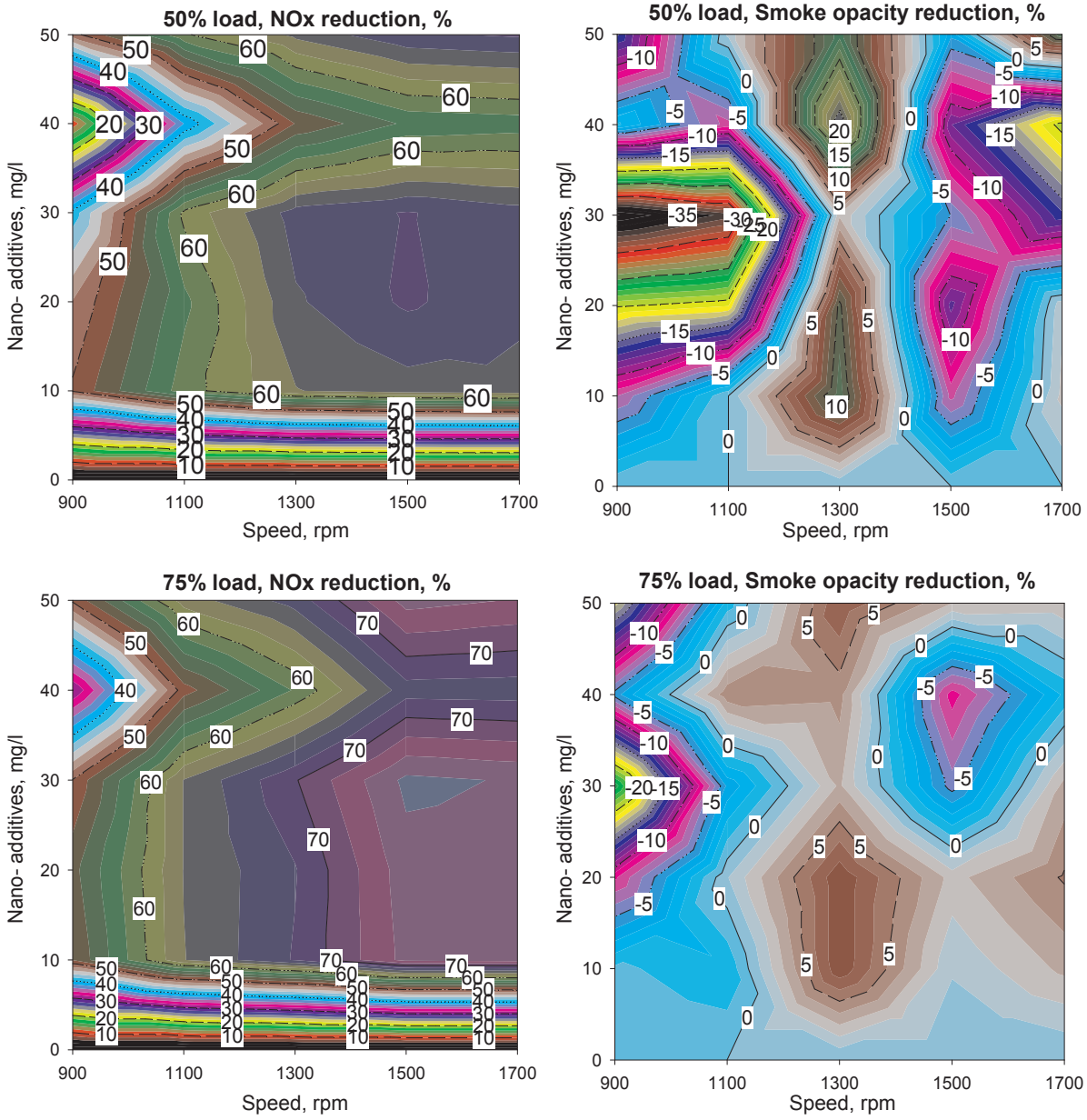

Fig. 18. The percentage reduction of engine NO_x and smoke opacity emissions at different engine loads and speeds.

irrespective of the engine speed, owing to the global mixture in the engine cylinder being very lean. While at high engine load and high speed, where insufficient oxygen to completely burn larger amounts of fuel will reduce the oxidation of carbon compounds to CO_2, and thus higher concentrations of CO were formed. Using JB20D blended fuel resulted in a remarkable increase in both CO and UHC emissions compared to diesel fuel. This effect is attributed to the higher viscosity of JME which causes poorer fuel atomization, resulting in prolonged ignition delay. Another reason may be attributed to the improper combustion of layers adjacent to the cylinder wall. These layers would contain a larger fraction of hydrocarbons which have escaped from the denser and longer-penetrated fuel spray in case of JB20D, and thus more UHC were emitted in the exhaust gases. These results were comparable with that found by Huzayyin et al. [16] and Shehata and Abdel-Razek [15].

From Fig. 16, it can be observed that the Al_2O_3 additives have a remarkable positive effect on CO and UHC emissions. This could be probably due to the higher surface to volume ratio, high catalytic activity and enhanced fuel-air mixing in the combustion chamber, resulting in shortened ignition delay. Generally, irrespective of the value of nanoparticles concentration, the CO and UHC emissions were lower than those emitted when either diesel fuel or JB20D fuel blend was used. The maximum reduction in CO and UHC emissions were attained at the dose level of 20–30 mg/l. These results were matched with findings of Ganesh and Gowrishankar [54], Selvan et al. [28], and Basha and Anand [33].

6. Recommendations of Al_2O_3 nanoparticles dose level

Figs. 17–19 show the summary of the results indicating the impact of adding Al_2O_3 into JB20D compared to pure JB20D blended fuel on the engine performance and emissions characteristics. The results show that the maximum reduction in bsfc by up to 12% was recorded at the dose level of 30–40 mg/l as represented in Fig. 17. From Figs. 18 and 19, it can be observed that at 50% load the maximum reduction in NO_x was by 60%, CO by 70%, UHC by 50%, and smoke opacity by 20%, which was obtained at the dose level of 20–40 mg/l. While at 75% load the highest emission reductions were as follows: NO_x by 70%, CO by

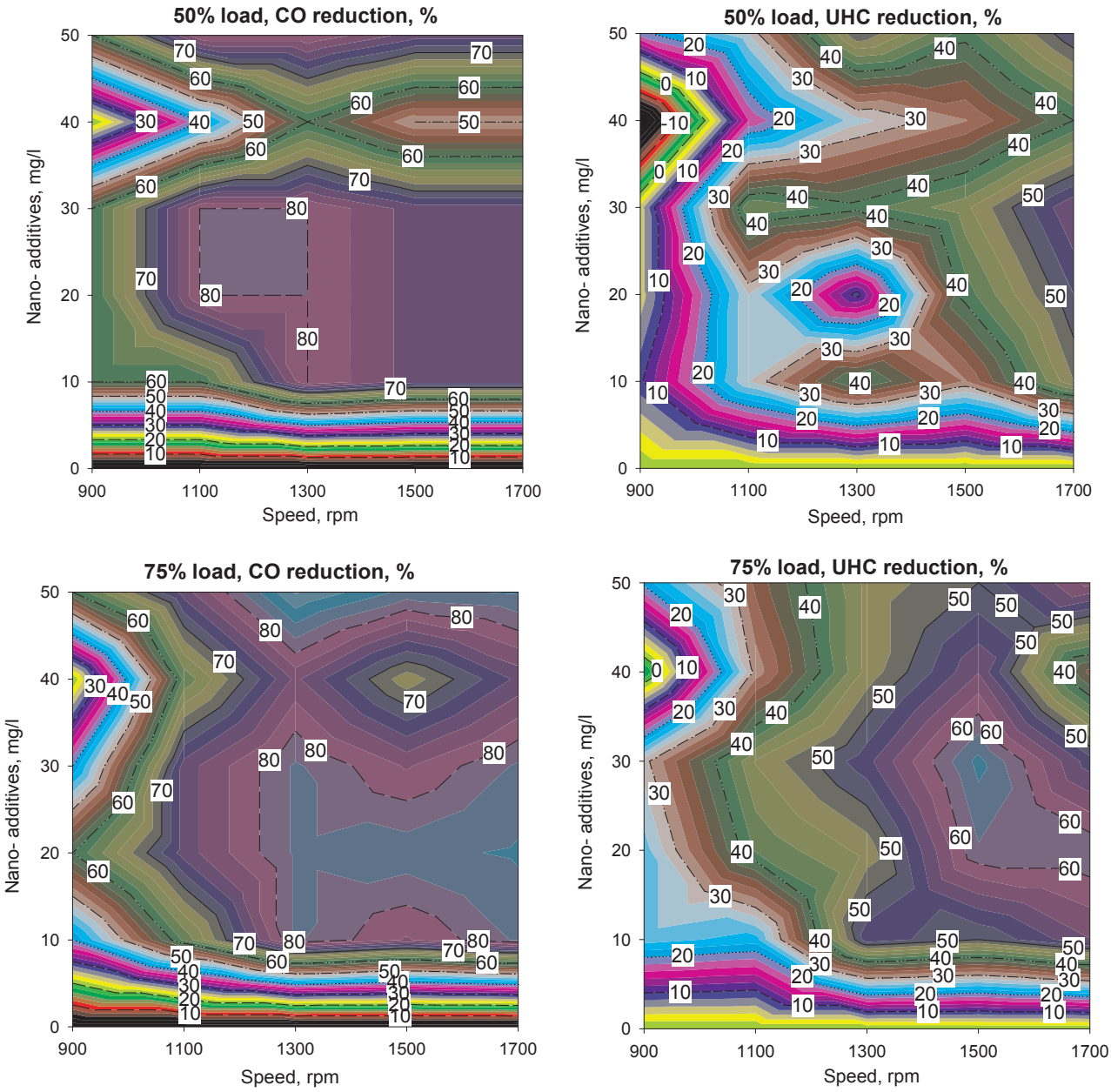

Fig. 19. The percentage reduction of engine CO and UHC emissions at various engine loads and speeds.

80%, UHC by 60%, and smoke opacity by 15%, which was obtained at the concentration of 20–40 mg/l. Furthermore, from combustion characteristics discussion in Section 5.1, it can be concluded that the maximum improvement in p_{max}, $dp/d\theta_{max}$, and $dQ_g/d\theta_{max}$ were obtained at the Al_2O_3 concentration of 30–40 mg/l. From the results of the whole investigation, it is necessary to select only one concentration of Al_2O_3 nanoparticles. Accordingly, during the selection process, the following features should be considered.

- Nanoparticles concentration should lead to optimal performance, or at least dosage should not deteriorate the mechanical performance of the diesel engine.
- Nanoparticles concentration should have the best improvement on engine emissions characteristics to achieve new emission norms.
- The dose level that may satisfy the above conditions should be of small value such that the mixture stability, the cost paid for dispersion process and cost paid for nanoparticles are kept the minimum.

The last point is critical to keep mixture uniformity and to reduce any negative effect of nanoparticles on engine components. In accordance to that and by comparing the overall effect of Al_2O_3 additives, it can be concluded that the concentration of 30 mg/l gave the best overall mechanical engine performance and the engine emissions characteristics simultaneously.

7. Conclusion

The experimental study was conducted on a single cylinder direct injection diesel engine at different speeds and load conditions to obtain the optimum concentration of Al_2O_3 additives into JB20D blend based on the evaluation of engine performance and emissions. Based on this investigation, the following conclusions were obtained:

1. The addition of Al_2O_3 nanoparticles into the JB20D blended fuel resulted in higher peak cylinder pressure, pressure rise rate and gross heat release rate as compared to pure JB20D.

2. Engine performance tests showed a remarkable increase in brake thermal efficiency by up to 15% and bsfc was decreased by up to 12% with the addition of Al_2O_3.
3. Emissions of NO_x, CO, UHC, and smoke opacity with the addition of Al_2O_3 into JB20D were significantly decreased by up to 70%, 80%, 60% and 35%, respectively as compared to JB20D.
4. The best mechanical performance was obtained at the Al_2O_3 concentration of 40 mg/l (bsfc was reduced by 12%, p_{max} was increased by 4.5%, $dp/d\theta_{max}$ by 4%, and $dQg/d\theta_{max}$ by 4%). While the maximum reduction in engine emissions was obtained at the dose level of 20 mg/l (NO_x was reduced by 70%, CO by 80%, UHC by 60% and smoke opacity by 35%).
5. The recommended Al_2O_3 concentration to obtain the remarkable enhancement in engine performance and emission was 30 mg/l.

This study recommends the nanoparticles concentration that improved the engine performance and emissions when fueled by Al_2O_3-JB20D blended fuels. This improvement helped in increasing the biodiesel blending ratio in the biodiesel-diesel blended fuels and reduced the energy and environmental problems resulting from the use of fossil fuels. During the current work, which lasted approximately two months, erosive effects of the Aluminium oxide on the engine fuel injection and exhaust system were not observed. However, long-term investigations on the life of the engine exhaust manifold and fuel injection system are needed to determine such effects.

Acknowledgments

Authors gratefully acknowledge Benha University for the support in providing the test facilities and instrumentations at the labs of Mechanical Engineering Department – Benha Faculty of Engineering, as well as financial support for the fuel preparation and properties measurements. Special thanks are due to Prof. M.S. Shehata, Prof. Ahmad E. Hassaneen, Dr. Radwan M. El-Zoheiry, Dr. Meshack Hawi and Eng. Belal Y. Ibrahim for their various support of this work.

References

[1] Hasan MM, Rahman MM. Performance and emission characteristics of biodiesel–diesel blend and environmental and economic impacts of biodiesel production: a review. Renewable Sustainable Energy Rev 2017;74:938–48. http://dx.doi.org/10.1016/j.rser.2017.03.045.
[2] Demirbas A. Political, economic and environmental impacts of biofuels: a review. Appl Energy 2009;86:S108–17. http://dx.doi.org/10.1016/j.apenergy.2009.04.036.
[3] Tamilselvan P, Nallusamy N, Rajkumar S. A comprehensive review on performance, combustion and emission characteristics of biodiesel fuelled diesel engines. Renewable Sustainable Energy Rev 2017;79:1134–59. http://dx.doi.org/10.1016/j.rser.2017.05.176.
[4] Ramkumar S, Kirubakaran V. Biodiesel from vegetable oil as alternate fuel for C.I engine and feasibility study of thermal cracking: a critical review. Energy Convers Manage 2016;118:155–69. http://dx.doi.org/10.1016/j.enconman.2016.03.071.
[5] Ramalingam S, Rajendran S, Ganesan P. Performance improvement and exhaust emissions reduction in biodiesel operated diesel engine through the use of operating parameters and catalytic converter: a review. Renewable Sustainable Energy Rev 2018;81:3215–22. http://dx.doi.org/10.1016/j.rser.2017.08.069.
[6] Atabani AE, César ADS. *Calophyllum inophyllum* L. – a prospective non-edible biodiesel feedstock. Study of biodiesel production, properties, fatty acid composition, blending and engine performance. Renewable Sustainable Energy Rev 2014;37:644–55. http://dx.doi.org/10.1016/j.rser.2014.05.037.
[7] Agarwal AK. Biofuels (alcohols and biodiesel) applications as fuels for internal combustion engines. Prog Energy Combust Sci 2007;33:233–71. http://dx.doi.org/10.1016/j.pecs.2006.08.003.
[8] El-Mogy NS. Egyptian experience in planting Jojoba. In: Fourth Int Water Technol Conf IWTC 99, Alexandria, Egypt; 1985. p. 431–5.
[9] El Moguy N. Jojoba: the green gold hope for the Egyptian desert development United Nations: economic and social commission for Western Asia. In: Report of the Experts Group Meeting Manama (Bahrain); 2002.
[10] Abu-Arabi MK, Allawzi MA, Al-Zoubi HS, Tamimi A. Extraction of jojoba oil by pressing and leaching. Chem Eng J 2000;76:61–5. http://dx.doi.org/10.1016/S1385-8947(99)00119-9.
[11] Abdel M, Farag HA, Ossman ME. Production of biodiesel from non-edible oil and effect of blending with diesel on fuel properties. Eng Sci Technol Int J 2012;2:583–91.
[12] Radwan MS, Ismail MA, Elfeky SMS. Jojoba methyl ester as a diesel fuel substitute: preparation and characterization. Appl Therm Eng 2007;27:314–22. http://dx.doi.org/10.1016/j.applthermaleng.2006.08.004.
[13] Selim MYE, Radwan MS, Saleh HE. Improving the performance of dual fuel engines running on natural gas/LPG by using pilot fuel derived from jojoba seeds. Renewable Energy 2008;33:1173–85. http://dx.doi.org/10.1016/j.renene.2007.07.015.
[14] Selim MYE, Radwan MS, Elfeky SMS. Combustion of jojoba methyl ester in an indirect injection diesel engine. Renewable Energy 2003;28:1401–20. http://dx.doi.org/10.1016/S0960-1481(02)00225-2.
[15] Shehata MS, Razek SMA. Experimental investigation of diesel engine performance and emission characteristics using jojoba/diesel blend and sunflower oil. Fuel 2011;90:886–97. http://dx.doi.org/10.1016/j.fuel.2010.09.011.
[16] Huzayyin AS, Bawady AH, Rady MA, Dawood A. Experimental evaluation of Diesel engine performance and emission using blends of jojoba oil and Diesel fuel. Energy Convers Manage 2004;45:2093–112. http://dx.doi.org/10.1016/j.enconman.2003.10.017.
[17] Saleh HE. Experimental study on diesel engine nitrogen oxide reduction running with jojoba methyl ester by exhaust gas recirculation. Fuel 2009;88:1357–64. http://dx.doi.org/10.1016/j.fuel.2009.01.023.
[18] Al-widyan MI, Al-muhtaseb MA. Experimental investigation of jojoba as a renewable energy source. Energy Convers Manage 2010;51:1702–7. http://dx.doi.org/10.1016/j.enconman.2009.11.043.
[19] Basu S, Miglani A. Combustion and heat transfer characteristics of nanofluid fuel droplets: a short review. Int J Heat Mass Transf 2016;96:482–503. http://dx.doi.org/10.1016/j.ijheatmasstransfer.2016.01.053.
[20] Attia AMA, El-Seesy AI, El-Batsh HM, Shehata MS. Effects of alumina nanoparticles additives into Jojoba methyl ester-diesel mixture on diesel engine performance. ASME 2014. http://dx.doi.org/10.1115/IMECE2014-39988.
[21] Shaafi T, Sairam K, Gopinath A, Kumaresan G, Velraj R. Effect of dispersion of various nanoadditives on the performance and emission characteristics of a CI engine fuelled with diesel, biodiesel and blends – a review. Renewable Sustainable Energy Rev 2015;49:563–73. http://dx.doi.org/10.1016/j.rser.2015.04.086.
[22] El-seesy AI, Abdel-rahman AK, Bady M, Ookawara S. Performance, combustion, and emission characteristics of a diesel engine fueled by biodiesel-diesel mixtures with multi-walled carbon nanotubes additives. Energy Convers Manage 2017;135:373–93. http://dx.doi.org/10.1016/j.enconman.2016.12.090.
[23] El-Seesy AI, Hassan H, Ookawara S. Effects of graphene nanoplatelet addition to jatropha Biodiesel-Diesel mixture on the performance and emission characteristics of a diesel engine. Energy 2018;147:1129–52. http://dx.doi.org/10.1016/j.energy.2018.01.108.
[24] Saxena V, Kumar N, Saxena VK. A comprehensive review on combustion and stability aspects of metal nanoparticles and its additive effect on diesel and biodiesel fuelled C.I. engine. Renewable Sustainable Energy Rev 2017;70:563–88. http://dx.doi.org/10.1016/j.rser.2016.11.067.
[25] Ganesh D, Gowrishankar G. Effect of nano-fuel additive on emission reduction in a Biodiesel fuelled CI engine. IEEE 2011:3453–9.
[26] Solero G. Experimental analysis of the influence of inert nano-additives upon combustion of diesel sprays. Nanosci Nanotechnol 2012;2:129–33. http://dx.doi.org/10.5923/j.nn.20120204.07.
[27] Gürü M, Karakaya U, Altıparmak D, Alıcılar A. Improvement of Diesel fuel properties by using additives. Energy Convers Manage 2002;43:1021–5. http://dx.doi.org/10.1016/S0196-8904(01)00094-2.
[28] Selvan VAM, Anand RB, Udayakumar M. Effects of cerium oxide nanoparticle addition in diesel and diesel-biodiesel-ethanol blends on the performance and emission characteristics of a CI engine. J Eng Appl Sci 2009;4:1–6.
[29] Sajeevan AC, Sajith V. Diesel engine emission reduction using catalytic nanoparticles: an experimental investigation. J Eng 2013:1–9. org/10.1155/2013/589382.
[30] Sajith V, Sobhan CB, Peterson GP. Experimental investigations on the effects of cerium oxide nanoparticle fuel additives on biodiesel. Adv Mech Eng 2010. http://dx.doi.org/10.1155/2010/581407.
[31] Kao M, Ting C-C, Lin B-F, Tsung T-T. Aqueous aluminum nanofluid combustion in diesel fuel. J Test Eval 2008;36:1–5. http://dx.doi.org/10.1520/JTE100579.
[32] Aalam CS, Saravanan CG. Effects of nano metal oxide blended Mahua biodiesel on CRDI diesel engine. Ain Shams Eng J 2015:0–7. http://dx.doi.org/10.1016/j.asej.2015.09.013.
[33] Basha JS, Anand RB. Effects of alumina nanoparticles blended jatropha biodiesel fuel on working characteristics of a diesel. Int J Ind Eng Technol 2010;2:53–62.
[34] Basha SJ, Anand RB, Basha JS, Anand RB, El Moguy N, Tewari P, et al. Role of nanoadditive blended biodiesel emulsion fuel on the working characteristics of a diesel engine. Renewable Sustainable Energy Rev 2011;3:173–89. http://dx.doi.org/10.1063/1.3575169.
[35] Basha JS, Anand RB. An experimental study in a CI engine using nanoadditive blended water-diesel emulsion. Fuel 2011:332–48. http://dx.doi.org/10.1080/15435075.2011.557844.
[36] Tyagi H, Phelan PE, Prasher R, Peck R, Lee T, Pacheco JR, et al. Increased hot-plate ignition probability for nanoparticle-laden diesel. Fuel 2008;2008.
[37] Gan Y, Qiao L. Evaporation characteristics of fuel droplets with the addition of nanoparticles under natural and forced convections. Int J Heat Mass Transf 2011;54:4913–22. http://dx.doi.org/10.1016/j.ijheatmasstransfer.2011.07.003.
[38] Mehta RN, Chakraborty M, Parikh PA. Nanofuels: combustion, engine performance and emissions. Fuel 2014;120:91–7. http://dx.doi.org/10.1016/j.fuel.2013.12.008.
[39] Thangavelu SK, Ahmed AS, Ani FN. Impact of metals on corrosive behavior of biodiesel-diesel-ethanol (BDE) alternative fuel. Renewable Energy 2016;94:1–9. http://dx.doi.org/10.1016/j.renene.2016.03.015.

[40] Venu H, Madhavan V. Effect of Al_2O_3 nanoparticles in biodiesel-diesel-ethanol blends at various injection strategies: performance, combustion and emission characteristics. Fuel 2016;186:176–89. http://dx.doi.org/10.1016/j.fuel.2016.08.046.
[41] Gumus S, Ozcan H, Ozbey M, Topaloglu B. Aluminum oxide and copper oxide nanodiesel fuel properties and usage in a compression ignition engine. Fuel 2016;163:80–7. http://dx.doi.org/10.1016/j.fuel.2014.09.008.
[42] Heywood JB. Internal combustion engine fundamentals. USA: McGraw Hill Series in Mechanical Engineering; 1988. doi: 10987654.
[43] Shehata MS. Cylinder pressure, performance parameters, heat release, specific heats ratio and duration of combustion for spark ignition engine. Energy 2010;35:4710–25. http://dx.doi.org/10.1016/j.energy.2010.09.027.
[44] Hohenberg GF. Advance approaches for heat transfer calculation. Soc Automot Eng SAE Tech Pap No. 790825; 1979. p. 2788–98.
[45] Stone R. Introduction to internal combustion engines. 2nd ed. Macmillan Press Ltd. J Chem Inf Model; 1989. doi: 10.1017/CBO9781107415324.004.
[46] Ghojel JI. Review of the development and applications of the Wiebe function: a tribute to the contribution of Ivan Wiebe to engine research. Int J Engine Res 2010;11:297–312. http://dx.doi.org/10.1243/14680874JER06510.
[47] Kline SJ. The purposes of uncertainty analysis. J Fluids Eng 1985;107:153–60.
[48] Oliveira JS, Montalvão R, Daher L, Suarez PAZ, Rubim JC. Determination of methyl ester contents in biodiesel blends by FTIR-ATR and FTNIR spectroscopies. Talanta 2006;69:1278–84. http://dx.doi.org/10.1016/j.talanta.2006.01.002.
[49] Shah M, Tariq M, Ali S, Guo QX, Fu Y. Transesterification of jojoba oil, sunflower oil, neem oil, rocket seed oil and linseed oil by tin catalysts. Biomass Bioenergy 2014;70:225–9. http://dx.doi.org/10.1016/j.biombioe.2014.08.029.
[50] Wang S, Li X, Wang S, Li Y, Zhai Y. Synthesis of γ-alumina via precipitation in ethanol. Mater Lett 2008;62:3552–4. http://dx.doi.org/10.1016/j.matlet.2008.03.048.
[51] Anna K, Leszek L, Episki K. Dispersion of ceria nanoparticles on γ-alumina surface functionalized using long chain carboxylic acids. Appl Surf Sci 2016. http://dx.doi.org/10.1016/j.apsusc.2016.12.127.
[52] EL-Seesy AI, Abdel-Rahman AK, Hassan H, Ookawara S, Hawi M. Investigation of the performance of a diesel engine fueled by biodiesel-diesel fuel mixture with addition of nanoparticles. In: Proc ASME 2017 Power Conf Jt With ICOPE-17 2017;1:1–9. doi: 10.1115/POWER-ICOPE2017-3055.
[53] Gupta HN. Fundamentals of internal combustion engines. 2nd ed. New Delhi: PHL Learning Private Limited; 2009. doi: 9788120328549.
[54] Ganesh D, Gowrishankar G. Effect of nano-fuel additive on emission reduction in a biodiesel fuelled CI engine. In: 2011 Int Conf Electr Control Eng ICECE 2011 – Proc; 2011. p. 3453–9. doi: 10.1109/ICECENG.2011.6058240.
[55] EL-Seesy AI, Abdel-Rahman AK, Bady M M, Ookawara S. The influence of multi-walled carbon nanotubes additives into non-edible biodiesel-diesel fuel blend on diesel engine performance and emissions. Energy Procedia 2016;100:166–72. http://dx.doi.org/10.1016/j.egypro.2016.10.160.